# REPORT DOCUMENTATION PAGE

AFRL-SR-AR-TR-05-



0114

| 1. AGENCY USE ONLY ( Leave Blank) | 2. REPORT DATE | 3. REPORT TYPE AND DATES COVERED |
|---|---|---|
| | 03 MAR 05 | FINAL REPORT – 15 JAN 02 THRU 14 SEP 04 |

4. TITLE AND SUBTITLE

**OPTICAL CDMA SYSTEMS IN HIGH-SPEED TELECOMMUNICATIONS**

5. FUNDING NUMBERS

**F49620-02-C-0021**

6. AUTHOR(S)

**XIAOWEI XIA, Ph.D.**

7. PERFORMING ORGANIZATION NAME(S) AND ADDRESS(ES)

**BOULDER NONLINEAR SYSTEMS, INC.**
**450 COURTNEY WAY, UNIT 107**
**LAFAYETTE, COLORADO 80026**

8. PERFORMING ORGANIZATION REPORT NUMBER

**FINAL REPORT**

9. SPONSORING / MONITORING AGENCY NAME(S) AND ADDRESS(ES)

**USAF, AFRL**
**AF OFFICE OF SCIENTIFIC RESEARCH**
**801 N. RANDOLPH ST, ROOM 732**
**ARLINGTON, VA 22203-1977**

10. SPONSORING / MONITORING AGENCY REPORT NUMBER

11. SUPPLEMENTARY NOTES

12 a. DISTRIBUTION / AVAILABILITY STATEMENT

**Approved for public release; distribution unlimited.**

12 b. DISTRIBUTION CODE

13. ABSTRACT (Maximum 200 words)

**BNS and the University of Colorado at Boulder developed a novel spectral optical code division multiple access (OCDMA) system with bipolar code capability for use in ultra-high-speed communication applications. By using liquid crystal spatial light modulators (SLMs), BNS and CU-Boulder have successfully fabricated and demonstrated a reconfigurable 2-user encoder-decoder system based on a fiber test-bed using three arrayed LC SLMs. A broadband Super Luminescent Diode source amplified by an EDFA has been spectrally encoded and decoded. The bipolar correlations of the codes are verified. Good contrast between the autocorrelation and cross correlation values shows that a binary information symbol can be recovered by an appropriate threshold operation. BER (bit-error-rate) measurements also show the ability of our system for MAI (multiple-access-interference) rejection. The system can be made very compact even with large numbers of subscribers when large format 2-D SLMs are used. Due to its programmability and two-dimensional operations in the optical domain, the system is suitable for implementing optically transparent routings in an ultra-fast Asynchronous Transfer Mode (ATM) switch.**

14. SUBJECT TERMS

**OPTICAL DCMA SYSTEM**
**HIGH-SPEED TELECOMMUNICATIONS**

15. NUMBER OF PAGES

**42**

16. PRICE CODE

N/A

| 17. SECURITY CLASSIFICATION OR REPORT | 18. SECURITY CLASSIFICATION ON THIS PAGE | 19. SECURITY CLASSIFICATION OF ABSTRACT | 20. LIMITATION OF ABSTRACT |
|---|---|---|---|
| **UNCLASSIFIED** | **UNCLASSIFIED** | **UNCLASSIFIED** | **UL** |

NSN 7540-01-280-5500

**Standard Form 298 (Rev.2-89)**
Prescribed by ANSI Std. 239-18
298-102

**BEST AVAILABLE COPY**

AFOSR STTR Phase II-Contract # F49620-02-C-0021

*Phase-II Final Report*

# Optical CDMA Systems in High-Speed Telecommunications

**Submitted to:**
**Air Force Organization of Scientific Research (AFOSR)**
**AFOSR/NM Room 713, 4015 Wilson Blvd, Arlington, VA 22203-1954**
**Program Manager: Dr. Jon Sjogren**
**Email: jon.sjogren@afosr.af.mil**

**Submitted by:**
**Boulder Nonlinear Systems**


**Technical Point of Contact:**
**Xiaowei Xia**
**Principal Investigator**
**xia@bnonlinear.com**

**Contractual Point of Contact:**
**Mark Tanner**
**Vice President**
**mtanner@bnonlinear.com**

# Table of Contents

# 1 Introduction

This document is the final report for the Air Force Office of Scientific Research (AFOSR) Phase II STTR contract (F49620-02-C-0021) awarded to Boulder Nonlinear Systems, Inc. (BNS). BNS proposed a spectral optical code division multiple access (OCDMA) system with bipolar code capability for use in ultra-high-speed communication applications. The proposed technology integrates multiple encoders for different users into a compact central unit, reducing overall system costs. A liquid crystal (LC) spatial light modulator (SLM), or a digital mirror device (DMD) can be used to spatially modulate the spectrum of the light source, which carries user signals. The advantage of the proposed system is that the spectral codes are reconfigurable. Each subscriber is able to communicate with all other subscribers. With its spectral bipolar code capability, the system can reject multiple access interference.

## 1.1 The Need for OCDMA

Recently, optical CDMA technology [1-3] has shown promise in optical communications, particularly in local-area optical fiber networks (LAN).[4] OCDMA technology allows a large number of users to share the entire channel bandwidth of an optical fiber network and offers asynchronous access. This is in contrast to optical time division multiple access (TDMA), which has very stringent synchronization requirements. OCDMA also has an advantage over wavelength division multiple access (WDMA), since it eliminates the need for a stable wavelength source and the need for ultrafast tunable sources and filters in future optical packet-switched networks.

In principle, any combination of spatial, temporal, frequency, and polarization information can be used for coding in OCDMA. There have been several different approaches proposed based on incoherent and coherent techniques. Coherent systems that utilize coherent superposition of fields have been studied by several groups.[1,2] For example, Weiner's group has assembled a simple fiber testbed [5] for an ultrashort pulse code-division multiple-access system, based on encoding and decoding of coherent ultrashort light pulses, in which multiple users share a common fiber medium by using different, minimally interfering optical code sequences. Recently, superstructured fiber-Bragg-grating technology has emerged as an attractive route to produce high-performance optical encoders and decoders.[6, 7] But, in all cases, picosecond or femtosecond pulsed lasers and phase detection systems are required, which are generally complex, expensive and cumbersome. Generally, coherent OCDMA systems also suffer from polarization and phase dependence, which require both polarization control and phase stabilization, and require setting and controlling optical delays on the scale of the optical wavelength in order to achieve the correct phases of superimposed fields.

Conversely, incoherent systems based on direct-detection reception, generally lack the bipolarity of coherent systems and are thus not as efficient at rejecting undesired signals

in the cross-correlation process.[8] Recently, however, some incoherent schemes implementing bipolar coding, as used in radio frequency CDMA and spread spectrum systems, were demonstrated.[9,10] Young's group[11] implemented a bipolar encoding scheme for coding the power spectrum of an erbium-doped superfluorescent fiber source using passive phase masks. However, the codes are not reconfigurable.

In this report, we present an incoherent and reconfigurable bipolar coding scheme of broadband light sources using liquid crystal (LC) Spatial Light Modulators (SLMs). The major advantage of this configuration is reconfigurable codes. With high-speed nematic LC such as dual-frequency nematic LC material, the reconfiguration speed can be fast (sub-ms), an advantage for many applications. In addition, the non-uniform spectral intensity distribution of the broadband light source means the coding patterns are not uniform. In principle, the length of the codes could be made longer by encoding more of the spectrum, allowing more users to be supported. This can be done by improving the uniformity of the source spectrum. Alternatively, uniform coding patterns can be obtained by adjusting the intensity of each spectral chip independently via independent adjustment of the driving voltage for each pixel of the SLM, i.e., by using an analog-driven LC SLM. Furthermore, wavelength scale distortion which can be a critical parameter in the correlation process [12] could be corrected actively by using an LC-SLM phase modulator.

## 1.2 Working Principles

Figure 1.1 illustrates the process of data transmission in an OCDMA scheme. Signals from all transmitters are distributed to every receiver using a star coupler. Each user receives all transmitted information, but is able to extract the signal of one particular transmitter from a background of multi-user interference using prior knowledge of the coding employed. Encoding and decoding processes are performed in the optical domain, eliminating any slowdown associated with optical-electronic conversion required in an electronic-based coding technology, a key motivation behind much of the work in OCDMA.

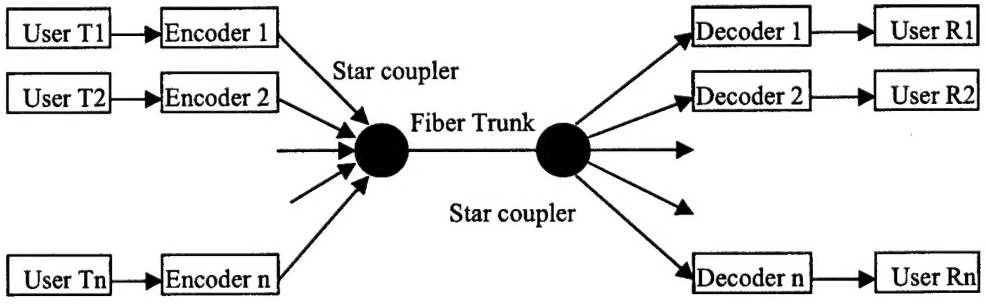


**Fig. 1.1: Optical CDMA local area network**

One of the great challenges in designing OCDMA systems is selecting a set of optical address codes that have low periodic cross-correlation. The most common codes used to achieve this goal are prime codes and optical orthogonal codes (OOCs).[13] However,

these codes suffer from high cross-correlation peaks compared to conventional bipolar codes, such as Gold, Kasami, and Hadamard codes. The bipolar nature of the codes is essential to achieving low cross correlations and low multiple access interference. It is also important to select optimum bipolar codes with good or tolerable correlation properties to achieve the best system performance. We use liquid crystal SLMs to encode the power spectrum of a broadband source into bipolar Walsh codes for data modulation. The coding principle is the same as that described by Young's group[10] representing a bipolar code with two unipolar codes as shown in Figure 1.2. A unipolar supercode J of length 2N is formed by concatenating a sequence code U and its complement, $U \oplus \overline{U}$. Each element of J is composed of

$$J(i) = \begin{cases} U(i), & 0 \le i \le N-1 \\ \overline{U}(i-N), & N \le i \le 2N-1. \end{cases} \qquad (1.1)$$

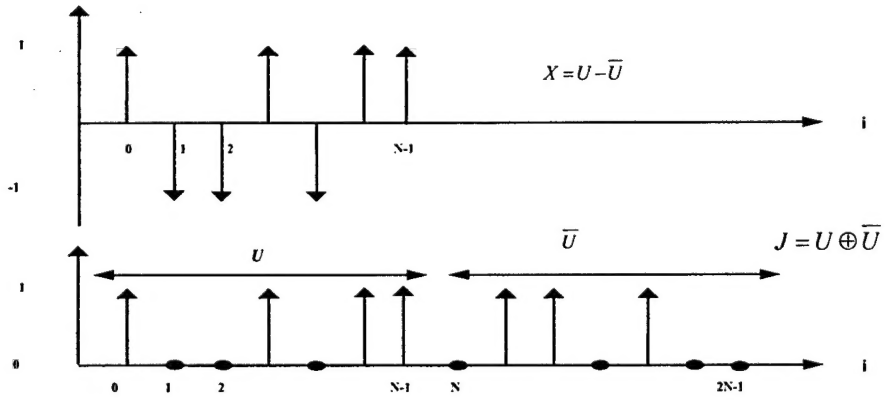


**Fig. 1.2: Bipolar conversion of a uniploar code.**

Figure 1.3 shows that a spectral amplitude pattern can be used to generate supercode J in the spectral domain.

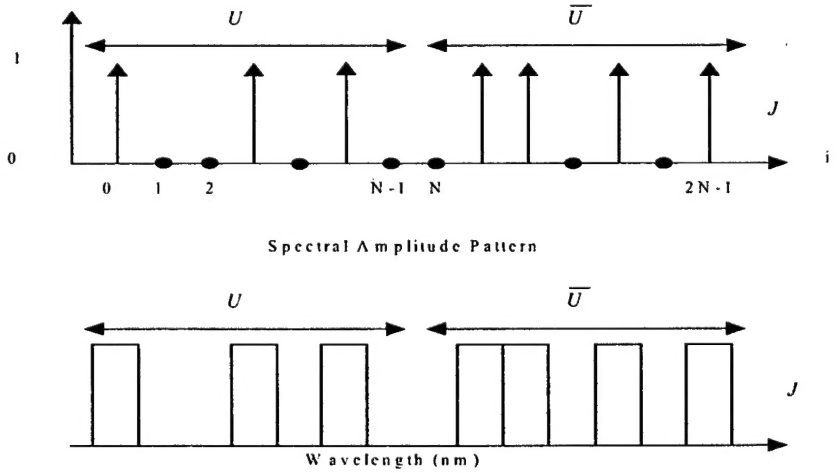


**Figure 1.3: Bipolar code implementation in an incoherent optical system.**

The key to system performance depends on constructing a decoder that implements a true bipolar correlation using only unipolar signals and intensity detection. This can be accomplished using two unipolar correlations, followed by a subtraction. [12] Let us consider two bipolar codes X and Y converted from their corresponding unipolar sequences U and V, and their unipolar supercodes $J = U \oplus \overline{U}$ and $K = V \oplus \overline{V}$. Since $X(i) = U(i) - \overline{U}(i)$ and $Y(i) = V(i) - \overline{V}(i)$, the zero-shift cross correlation of X and Y is

$$\begin{aligned}\Theta_{XY} &= \sum_{i=0}^{N-1} X(i)Y(i) = \sum_{i=0}^{N-1}\left[U(i) - \overline{U}(i)\right]\left[V(i) - \overline{V}(i)\right] \\ &= \sum_{i=0}^{N-1}\left[U(i)V(i) + \overline{U}(i)\overline{V}(i)\right] - \sum_{i=0}^{N-1}\left[U(i)\overline{V}(i) + \overline{U}(i)V(i)\right]. \qquad (1.2) \\ &= \sum_{i=0}^{2N-1}\left[J(i)K(i)\right] - \sum_{i=0}^{2N-1}\left[J(i)\overline{K}(i)\right] = J \cdot K - J \cdot \overline{K}\end{aligned}$$

The operations $J \cdot K$ and $J \cdot \overline{K}$ are unipolar correlations and can be performed optically, as described in the encoder/decoder system in Chapter 3. Therefore, a true bipolar correlation $\Theta_{XY}$ can be implemented using only unipolar signal intensity detection via Eq. (1.2).

## 1.3 Phase II Tasks

We proposed in Phase II to build a prototype one-dimensional spectra-coded OCDMA system for application in high-speed telecommunications. The proposed technology is based on our research results from Phase I, where we implemented a conceptual demonstration of an optical CDMA system with bipolar coding capacity. The tasks in Phase II involved design and fabrication of analog controlled arrayed LC SLMs; construction of prototype one-dimensional encoder and decoder system; algorithm development and system simulation; system integration and full testing.

We successfully constructed in Phase II a prototype OCDMA system. Our system is based on a fiber test-bed, that is, the signal is coupled in and out of the system by optical fibers. This makes the system compact and easy to install for fiber optical communications. A 30-nm broadband Superluminesent Diode (SLD) amplified by an erbium-doped fiber amplifier (EDFA) was used as the information source. We tested the encoding/decoding capability by measuring the auto- and cross-correlations, multiple-access-interference (MAI) and the bit-error-rate (BER) performance under different circumstances.

## 1.4 Structure of the Final Report

This report is organized as following. Following this introductory chapter, we will discuss general technical operation of liquid crystals and various details for the design and fabrication of arrayed LC SLMs. In Chapter 3, construction of our OCDMA system will be described and various testing results reported. These include the system configuration, spectral encoding and decoding, measurements for auto- and cross-correlations, multiple-access-interference (MAI) rejection, bit-error-rate (BER). In Chapter 4, we analyze the noise performance of the OCDMA system. The major achievements of phase II will be summarized in Chapter 5. Finally, technical references are listed, attached along with our two publications on SPIE proceedings resulting from this STTR project.

# 2 Development of Arrayed LC SLMs

Liquid crystal optical modulators [14, 15] offer several advantages including large modulation depth, inertia-less switching, low power dissipation, potential for large aperture operation, and low cost. LC modulators can also provide a variety of optical transmittance (reflectance) characteristics. LC devices can achieve different types of modulation including bipolar, real-axis, phase-only, coupled phase-amplitude and broadband phase shifting. This versatility is an additional advantage in today's atmosphere of budget constraints where multipurpose modulators are sought as a cost effective means to implement different subsystems. The various optical transmittance (reflectance) characteristics of LC modulators depend on the modulator architecture and the LC material used, as does the response time. Response times can range from several ms to 1 μs. The key components in our OCDMA system are the three arrayed LC SLMs used for spectral coding modulation. This chapter describes the various details related to the successful fabrication of arrayed SLMs.

## 2.1 Technical Background: Liquid Crystal Physics

Liquid crystals (LCs) have a fluid-like nature, but the molecules exhibit structural order. The electro-optic properties of the fluid arising from the structural order resemble the properties of solid crystals. For the most common type of LC, temperature alters the structural nature of the LC producing distinct LC phases. Thermotropic is the classification given to this type of LC. For thermotropic compounds, there are three possible LC phases, referred to as nematic, cholesteric and smectic. Most electro-optic devices use thermotropic LC since this material allows light to be modulated using low-amplitude voltages. However, it is possible to freeze these ordered phases into a permanent state using an UV crosslinkable polymer host making the ordered structure non-thermotropic. These solid films are useful as passive components such as waveplates or filters.

### 2.1.1 Nematic Liquid Crystal

For nematic LC phase retarders, the preferred alignment is a zero-twist (or parallel) alignment. In such an alignment, the LC molecules (which are cigar shaped) all lay parallel to the substrate surface and all the molecules point in the same direction. For example, consider a deep cigar box sitting on a table with all the cigars aligned in one direction held in place by the sides of the box. This is similar to the LC cell, except there are no sides to the box (only a top and bottom which corresponds to the substrates). The cigar shaped molecules stay in place because of the grooves placed in the alignment layer on the substrate surface. The molecules at the surface are anchored in place by these grooves and the internal molecules follow the surface molecules because this is an

electrically neutral arrangement. If we apply a voltage across the cell, we upset the electrical balance and the molecules rotate in the field, finding another state where forces are again balanced.

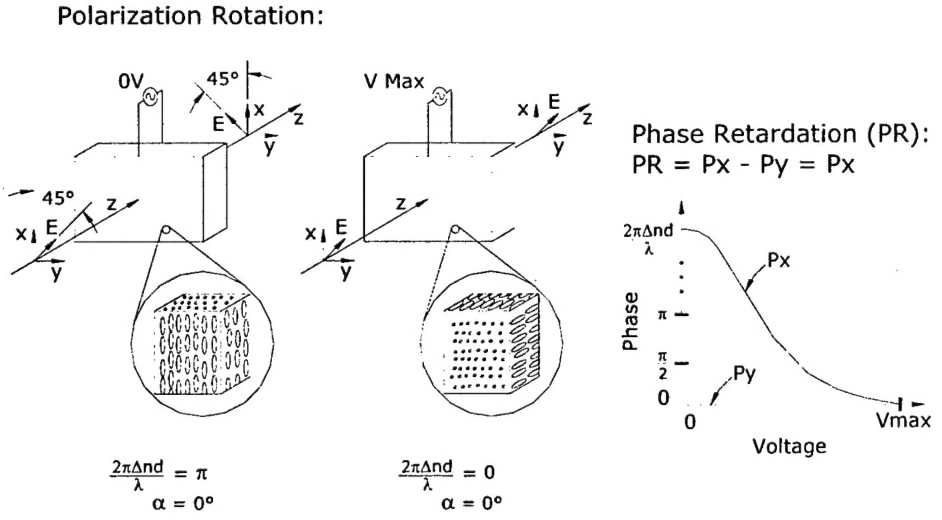


**Fig. 2.1: Nematic LC phase retarder showing molecular structure for energized and non-energized states as well as its modulation characteristics. The graph shows the phase retardation (PR) between the x and y E-field components where Px and Py represent the phase variation of each field component, respectively.**

As the cigar-shaped molecules rotate, the optical properties of the cell change. The cigar shape of the molecules causes this difference to occur. When the light propagates through a LC cell, it travels faster through the cell when the light's polarization (i.e. direction of the E-field) is perpendicular to the long axis of the LC molecule. In Fig. 2.1, this is the Y-component of the E-field. This faster propagation is relative to when the polarization direction of the light is parallel with the long axis of the molecule (i.e. the X-component in Fig. 2.1). Therefore, light travels through the cell at different speeds depending on its polarization. One polarization of the light is retarded with respect to the other polarization, hence the name "retarder". The amount of phase retardation is related to the thickness of the LC cell, $d$, and the birefringence of the LC material, $\Delta n$, and the wavelength of the light, $\lambda$. For a parallel-aligned nematic, the cigar-shaped molecules are normally parallel with the surface of the substrates. As a voltage is applied across the cell, the molecules at the center of the cell rotate such that the molecule's long axis is perpendicular to the cell's electrode. For the device shown in Fig. 2.1, the long axes of the molecules align with the electric field directed along the Z-axis. This molecular rotation causes the light to travel through the cell at one speed regardless of polarization. That is, the cell becomes optically isotropic.

With this LC arrangement, it is possible to tune the cell from a maximum retardance value to virtually none. For a perfectly aligned cell, the retardance of the cell changes

continuously with the applied field, without changing the amplitude of the two orthogonal polarization components. Thus, a pure phase change occurs between the two polarization components. Phase purity is important for the polarization rotator and for a LC tunable filter to prevent cross coupling of the polarization components.

### 2.1.2 Smectic (Ferroelectric) Liquid Crystal

The smectic liquid crystal phase is characterized by a more ordered layered structure than the nematic phase. The ordered layered structure resembles bookshelves (refer to Fig. 2.2), where one row of cigar-shaped LC molecules is separated from the next row by planes running normal to the substrate's surface. Within the smectic layers (between the bookshelves), however, the molecules are positioned randomly. In 1975, Meyer [16] reported the existence of ferroelectricity in the tilted phase of smectic liquid crystals. One such tilted phase is smectic C (SmC*). For a chiral material, this tilted phase produces macroscopic polar order, as the molecules are inhibited in their rotation about the long axis. Therefore, the SmC* phase is ferroelectric, and this liquid crystal structure is commonly referred to as ferroelectric liquid crystal (FLC). For an FLC modulator, a vast improvement in switching speed results over switching speeds characteristic of nematic materials. The application of an electric field parallel to the smectic layers produces a first order coupling to the dipole moment, as opposed to the second order dielectric coupling associated with nematic switching. Typical switching speeds for FLC devices are tens of microseconds.

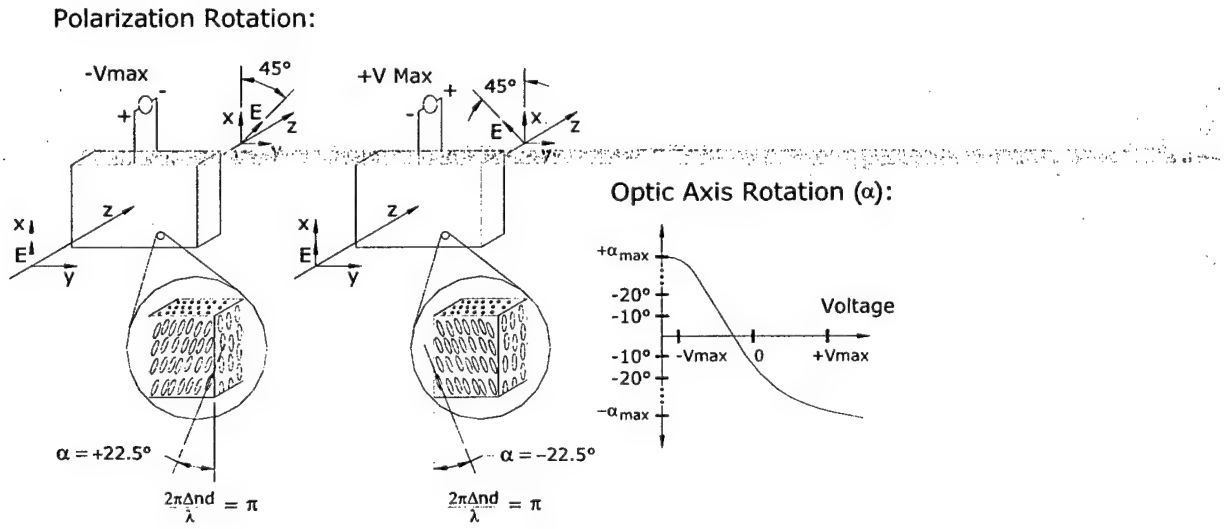


**Fig. 2.2: Ferroelectric LC modulator showing the molecular structure of the device for energized and non-energized states. The graph shows the optic axis rotation of the material, representing the effective angular tilt of the long axes of the molecules.**

As mentioned above, the smectic ordering restricts the molecular rotation. The long axis of the molecule does not freely rotate as it does in a nematic material. Instead, the long axis of the molecule stays semi-parallel with the surface, but has a tilt with respect to the smectic planes (refer to Fig. 2.1). As a voltage is applied, the tilt angle of the molecule changes, which also changes the effective optic axis of the material as shown in the graph of figure 2.2. However, the retardance of the cell remains constant. Therefore, the FLC structure acts as an electro-optically tunable waveplate. If the waveplate retardance equals a halfwave ($\pi$), then linearly polarized light is rotated through an angle that is twice the angle of the optic axis as shown in Fig. 2.2.

### 2.1.3 Cholesteric Liquid Crystal

Cholesteric liquid crystal has a structure that is similar to various compounds that contain cholesterol, hence the name. It is basically a nematic LC that has a helical structure. That is, the cigar-shaped molecules assemble into layers where the cigar shape rotates between layers instead of following one direction. This helical structure (refer to Figure 2.3) causes the material to act as a circular polarizer, which breaks randomly polarized light into right- and left-handed circularly polarized components. The component with the same handedness as the cholesteric LC is reflected when the wavelength falls within the selective reflection band and transmitted at other wavelengths (refer to the first plot in Figure 2.3). The component with the opposite handedness is transmitted at all wavelengths as shown in the second plot of Figure 2.3.

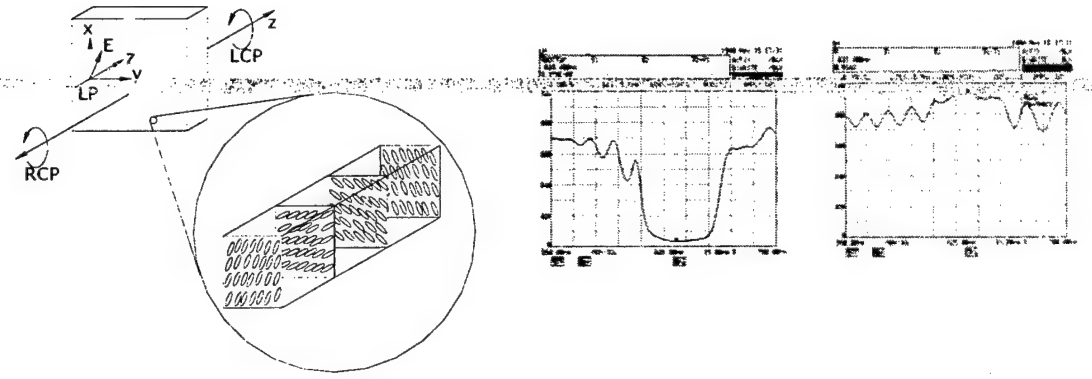


**Fig. 2.3: Cholesteric LC showing its molecular structure and how it chiral nature splits light into right and left-handed circularly polarized components. Two spectrum analyzer plots of a polymer cholesteric mirror fabricated by BNS where the circular handedness of the broadband light source is different for each plot. That is, the circularly polarized light from the source is either right handed (first plot) or left handed (second plot).**

### 2.1.4 Polymer Liquid Crystal

Nematic crosslinkable LC silicones can be fabricated into zero-order retarders on a single substrate by spin casting methods. The liquid crystal is converted into a permanent glass state using an ultra-violet (UV) cure. Currently, we use the polymer nematic LC and spin-cast fabrication technique for producing experimental broadband modulators.

The fabrication of polymer cholesteric LC films is similar to passive polymer nematic LC films. The primary difference is that the cholesteric LC is heat sensitive when in the liquid state. Heat changes the color of the material, which allows the material to be tuned to a different wavelength by controlling the heat of the sample while it is in a liquid state. When the polymer cholesteric LC is exposed to UV, the cholesteric LC molecules are locked into a glassy solid state by the side-chain polymers. The glass matrix formed by this polymerization freezes the pitch of the cholesteric LC making the selective reflection band nearly insensitive to temperature.

## 2.2 Liquid Crystal Modulators and Coding Patterns

BNS was among the first companies to introduce an SLM product based on single crystal silicon (VLSI) technology, and the first company to introduce a 10-KHz frame rate analog SLM of any kind. BNS has already developed four reflective SLMs based on silicon backplanes and converted them into successful products,[14, 15] including a 128x128 binary SLM, 256x256 binary SLM, 128x128 multi-level SLM, and most recently a 512x512 multi-level SLM, which is currently being re-designed to utilize newer foundry techniques to enable a smaller optical head and significantly improved light efficiency. Our current analog 512x512 SLM has a pixel pitch of 15 microns and BNS has begun investigation of our next generation 512x512 SLM with a 6-micron pixel pitch. All four were developed exclusively for use in the optical processing arena.

For the application of a one-dimensional OCDMA system, we use transmissive nematic 1x64 linear arrayed SLMs. The SLM has a pixel pitch of 110 μm and a pixel width of 100 μm. Twisted nematic LC material is used to fill the SLM, and gives greater than $\pi$ phase shift at 1.5-μm wavelength for full amplitude modulation. Each single or grouped (when 64 pixels are used, two pixels are grouped as one chip) chip is one bit, composing a 32-bit bipolar code made up of a 16-bit unipolar code and its complex conjugate. Three identical 1x64 SLMs have been fabricated and tested. They all give a $\pi$ phase shift for 1.5 μm light when driven at a holding voltage of about ±6V. The SLMs are driven by three separate electronic drivers controlled via a PC. A program using C++ has been produced to control the three drivers simultaneously through the PC, so that different patterns (corresponding to different optical codes) can be simultaneously chosen. The program can change parameters like code patterns, offset position, holding voltages etc. The control of offset position for coded patterns is necessary for accurate alignment of code patterns produced from two different SLMs.

Figure 2.4 shows a 90° twisted nematic (TN) LC structure inside a cell. In the 90° TN cell, the director of the back surface is twisted 90° with respect to the front surface when the TN LC is in the unenergized state. When linearly polarized light traverses through the TN LC cell, the plane of polarization follows the twist of the LC directors if the Mauguin's condition is satisfied, i.e., $d \cdot \Delta n >> \lambda$. Under this circumstance, the output beam remains linearly polarized except that its polarization axis is rotated by 90°. Figure 2.4 also shows that the directors of the 90° TN cell are perpendicular to the surfaces of the windows when the external electric field is applied. In this case, the plane of polarization will remain in its original orientation. With the output polarizer crossed in relation to the input polarizer, the light intensity can be switched on or off. The light signal can be encoded into various "cross" and "bar" patterns.

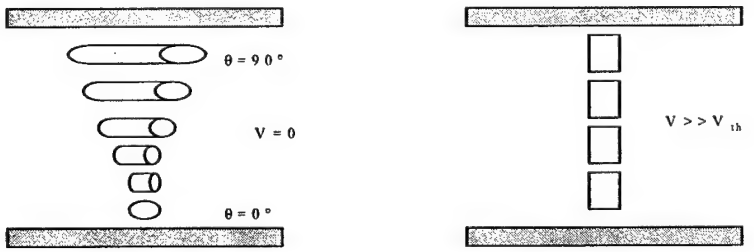


Fig. 2.4: Twisted nematic liquid crystal modulator.

## 2.3 Fabrication of Analog SLMs

Three 1x64 arrayed SLMs have been fabricated and tested. Detailed design and operation is described in the following.

### 2.3.1 Optics

The optical head consists of a Laser etched ITO backplane and cover glass filled with nematic liquid crystal. The SLM is connected to the Mount board using a flexible electrical cable called Elform. Figure 2.5(a) shows a side view of the SLM, and Figure 2.5(b) shows a top view of the SLM.

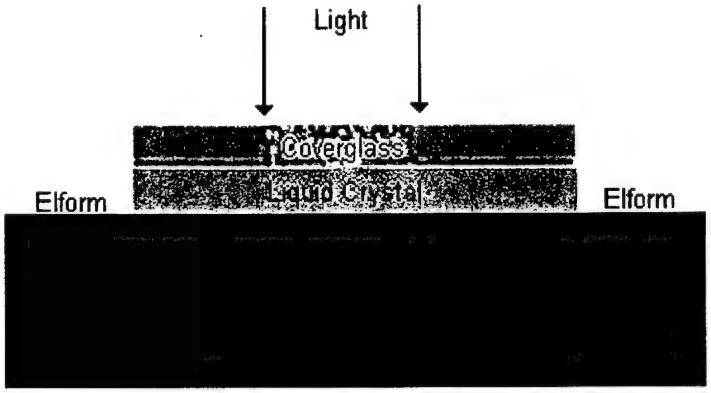


**Fig. 2.5(a): SLM side view**

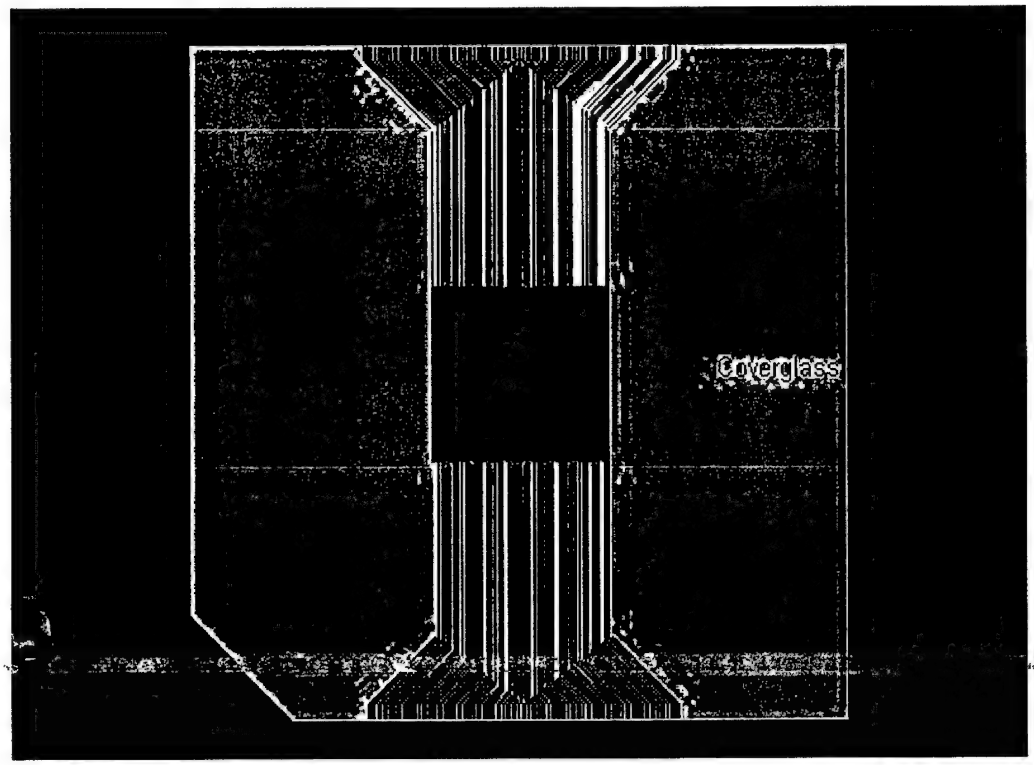


**Figure 2.5(b): SLM top view**

### 2.3.2 Hardware

To drive the 1x64 arrayed SLMs with a simple and compact "plug and play" driver, we have determined that the best interface for the driver board is the Universal Serial Bus (USB). We have successfully fabricated and assembled the USB interface, 64 channel driver boards. The board is 4″ x 4.75″ in size. This driver board interfaces with the USB port on the computer. Power is supplied to the board using a 5V wall plug. The output of the driver board is 64 analog channels with a maximum voltage of approximately +/-7V with a static coverglass voltage and +/-14V with coverglass flipping.

These 64 analog channels are sent out two 40-pin ribbon cables to a connector board, which will then connect to the liquid crystal device using Elform as the interconnect. The following block diagram (Figure 2.6) illustrates the architecture of the system.

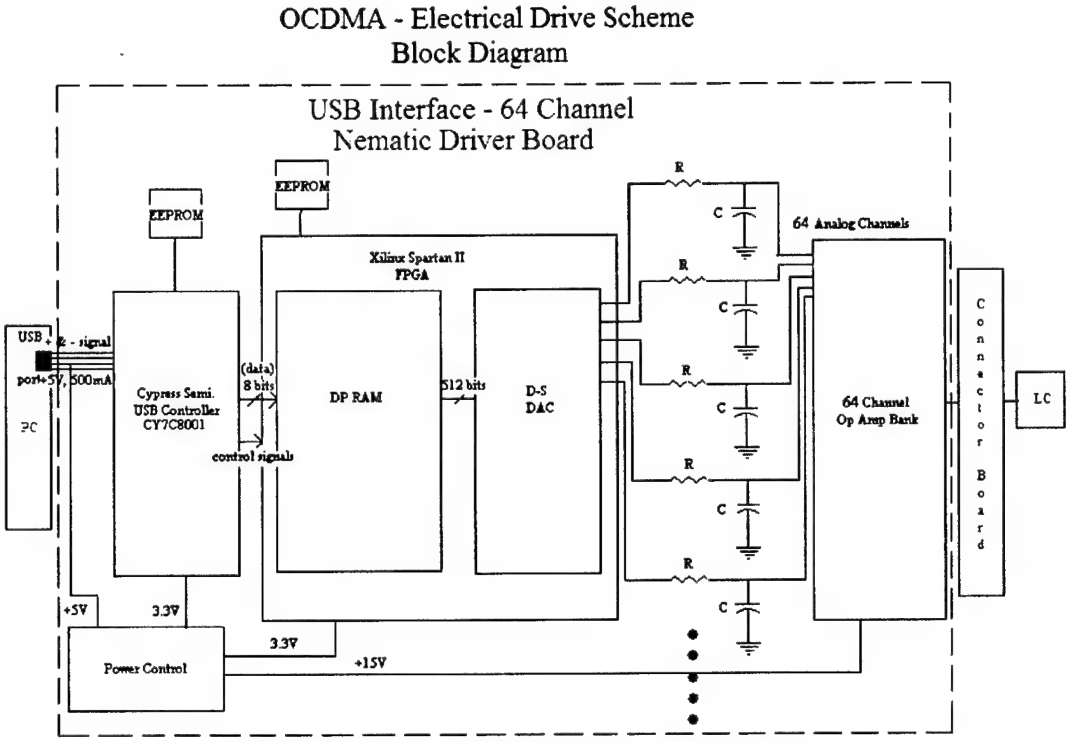


**Figure 2.6: Block diagram of the drive scheme.**

The image of Figure 2.7 is a picture of the USB interface – 64 Channel Nematic Driver Board. The connector in the lower left hand corner of the board is the USB receptacle, which connects to the computer using a USB cable. The connector in the upper left corner is the power supply receptacle. The two connectors on the right are 40-pin ribbon connectors that connect to a small connector board. Three USB drivers were built to drive three 1 x 64 linear array LC devices, respectively.

### 2.3.3 Software

The software application for the USB interface – 64 Channel driver board was also developed by BNS. This program allows the user to specify the state of the 64 pixels, and the voltage of each pixel for its high and low state. Figure 2.8 shows what the program looks like when first opened.

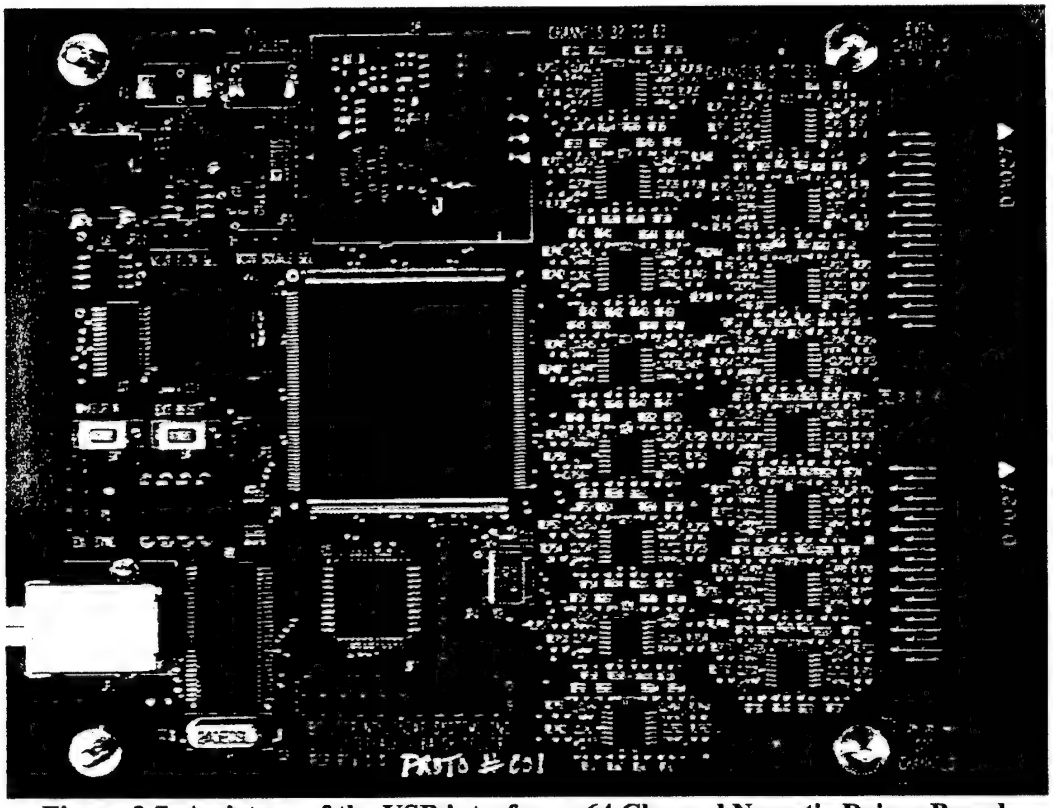

**Figure 2.7: A picture of the USB interface – 64 Channel Nematic Driver Board.**

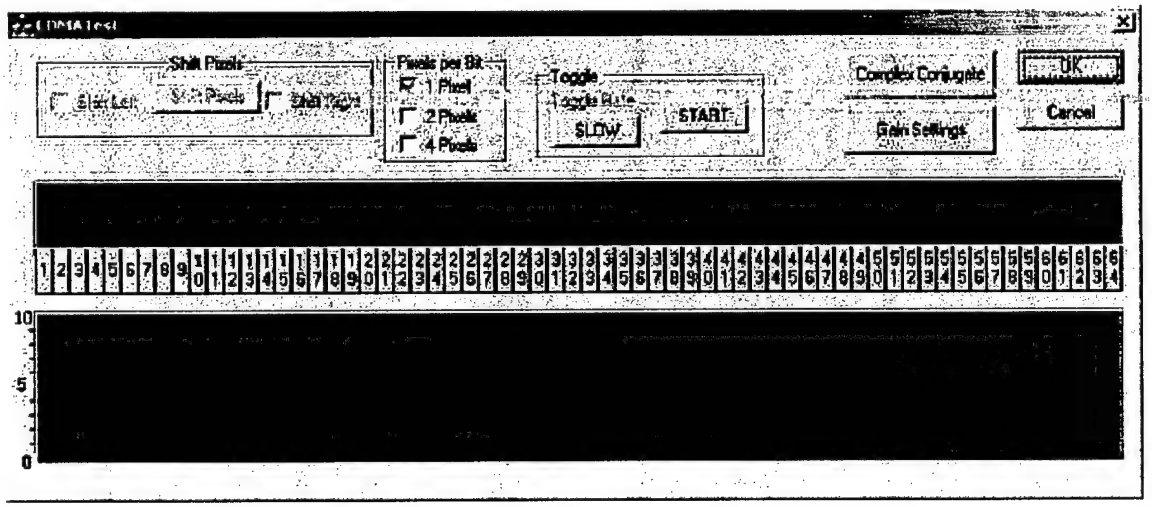


**Figure 2.8 CDMA Software package screen shot.**

Across the middle of Figure 2.8 there is a row of buttons. Each button controls the state

of one pixel. Thus, if button 1 is clicked, then pixel 1 would be set to either a high state or a low state depending on its current state. In other words, if pixel 1 is high, and the pixel 1 button is clicked, then the pixel state will switch to a low state. The space above each pixel button indicates the state of that pixel. So, in Figure 2.8, all of the spaces above the pixels are black, and are therefore in the low state. If the user were to click button 1, then the space above button 1 would turn white, and pixel 1 would be in the high state.

Below the row of buttons is a graph. The red line on the graph indicates the voltage of each pixel. If the user should want to change the voltage of a particular pixel, then the "Gain Settings" button should be clicked. This will bring up the dialog shown in Fig. 2.9.

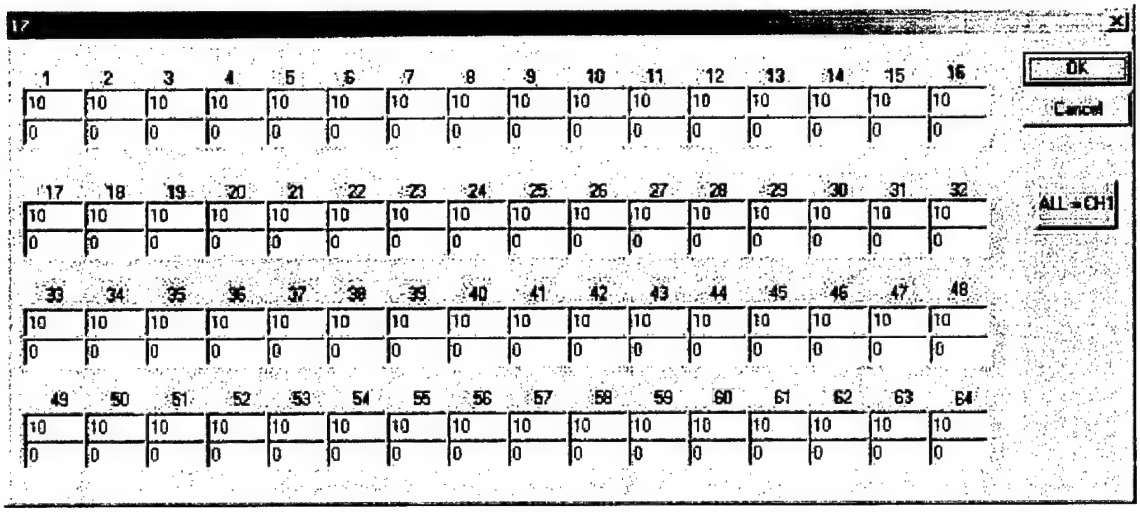


**Figure 2.9**

In Figure 2.9 there are edit boxes for the high and low state for each of the 64 pixels. Each pixel has two rows of edit boxes, the top row controls the voltage of the pixel when it is in its high state; likewise, the bottom row controls the voltage of the pixel when it is in its low state. Thus, by changing the values in these edit boxes the user will change the voltages applied to the pixels.

Returning back to Figure 2.8, there are a series of buttons across the top of the dialog box. Each of these buttons perform simple operations of the pixel states. So, starting on the left side of the dialog there is a shift pixels button. This will allow the user to shift the state of the pixels from either the right to the left, or from the left to the right depending on which checkbox is selected. The user should note that the pixels will wrap when shifting. Thus, if shift right is selected, then the state of pixel 64 will become the state of pixel 1. Likewise, if shift left is selected, then the state of pixel 1 will become the state of pixel 64.

The next pixel state function is "Pixels Per Bit". This function sets the number of pixels that each pixel button controls. In Figure 2.8 the "1 Pixel" option is selected. This

means that button 1 only controls the pixel state of pixel one. However, if the "2 Pixel" option is selected then the state of pixel 1 is tied to the state of pixel 2. Therefore, if either button 1 or button 2 is clicked then the state for both pixels will change. This is shown in Figure 2.10 and Figure 2.11.

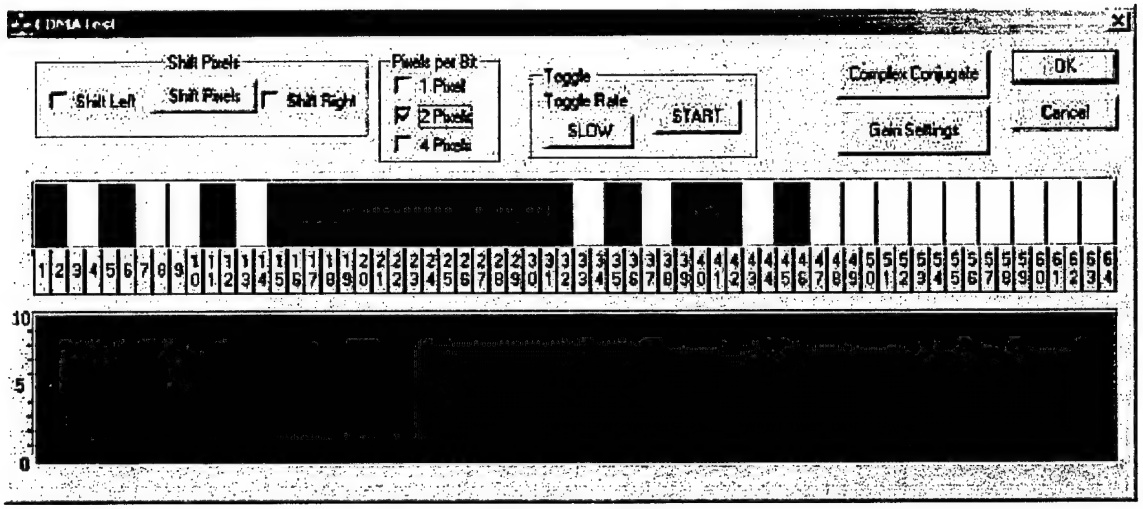


**Figure 2.10**

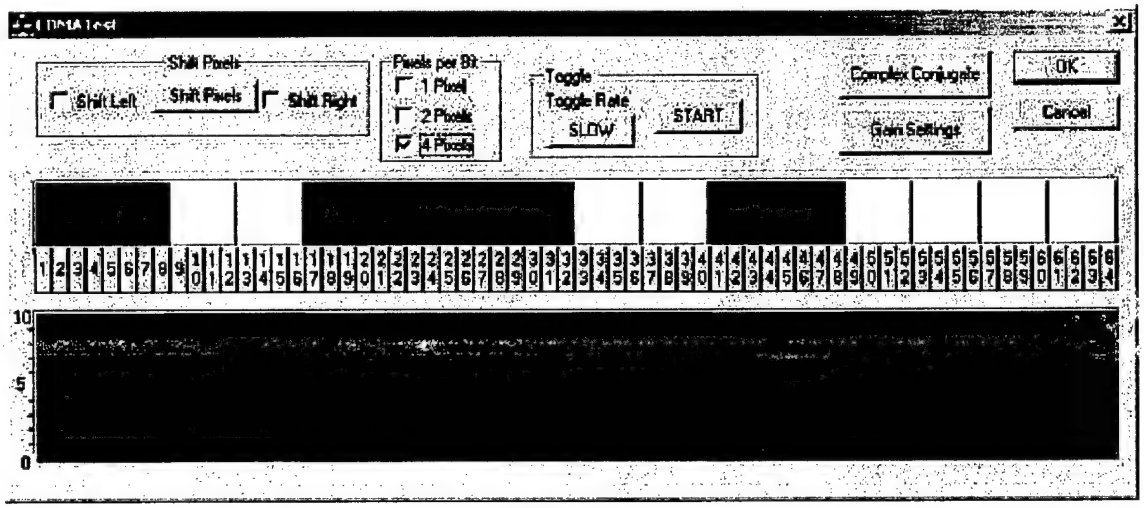


**Figure 2.11**

The next pixel state function is the "Toggle" function. This will toggle the state of the pixels at either a slow or fast rate. To change the toggle rate from slow to fast, or from fast to slow, click the "Toggle Rate" button. To start the pixels toggling, click the start button. This button will become a stop button when the pixels begin toggling, and should be used to stop the toggling.

The next pixel state function is the "Complex Conjugate" button. This will erase the state of pixels 33 through 64, and replace them with the complex conjugate of the state of

pixels 1 through 32. Figure 2.12 shows the state of the pixels prior to clicking the "Complex Conjugate" button, and Figure 2.13 shows the state of the pixels after clicking the "Complex Conjugate" button. Thus in Figure 2.13 the pattern for pixels 33 through 64 matches that of pixels 1 through 32, except that the pixel state of pixels 33 through 64 are inverted.

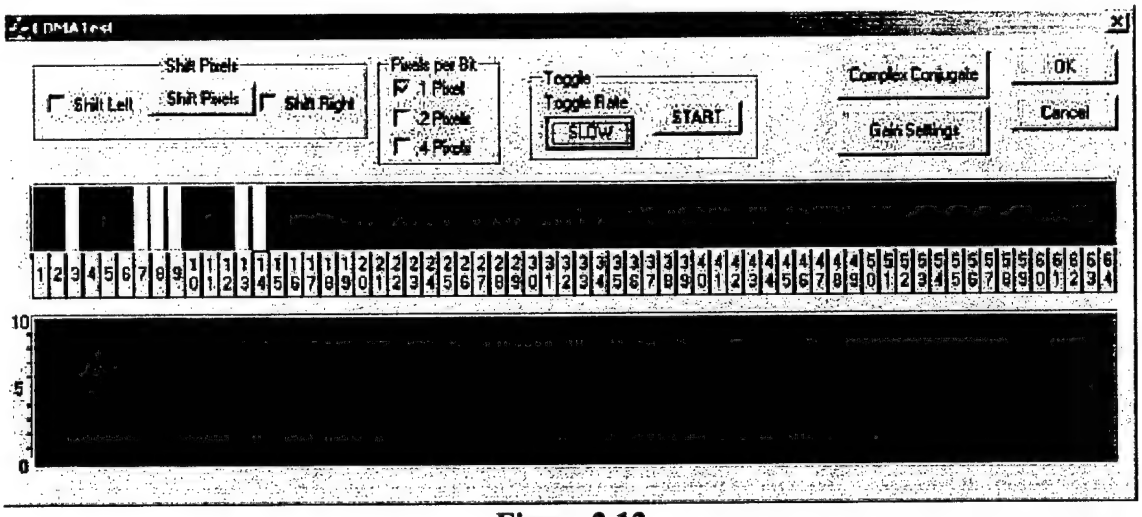


**Figure 2.12**

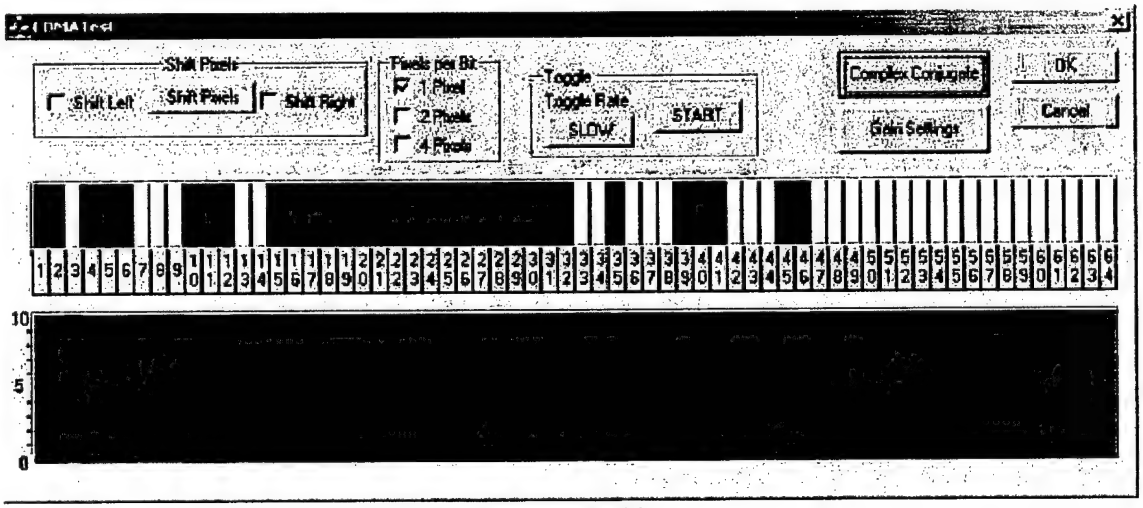


**Figure 2.13**

# 3 Prototype OCDMA System

## 3.1 Spectrum Encoding

### 3.1.1 Implementation of Spectrum Encoding

Figure 3.1 shows an encoder setup to encode an optical signal with spectral bipolar codes. We address the code for each user in the spectrum domain by using a standard 4-f pulse shaping apparatus, composed of two gratings at the outer focal plane of a telescope. Single-mode optical fibers with appropriate collimators are used on all the light ports. The 1.5-μm Super Luminescent Diode (SLD) fiber output beam amplified via an erbium doped fiber amplifier (EDFA) is collimated via a GRIN lens (GL1) and diffracted by the grating (G1). The diffracted beam is collimated by a cylindrical lens (L1) of focal length 100 mm (with focal point at the grating). The collimated beam passes through the liquid crystal SLM that is between two crossed polarizers (P1 and P2). The pixelated liquid crystal elements are designed such that each wavelength channel can be driven independently. The coded channels are focused by the output lens (L2) and recombined by the output grating (G2) into a single beam that is coupled to output fiber via a GRIN lens (GL2). By adjusting the polarization direction of P1 and P2, and the holding voltage of the SLM, which determines the LC phase delay, the encoding contrast can be optimized. The modulated spectrum power can also be flattened by adjusting the driving voltages applied on each individual pixel of the SLM. Due to the space-frequency correspondence at the grating spread out, spatial modulation of the light beam leads to the modulation in spectral domain. Using this setup we are able to perform reconfigurable modulation of the light spectrum.

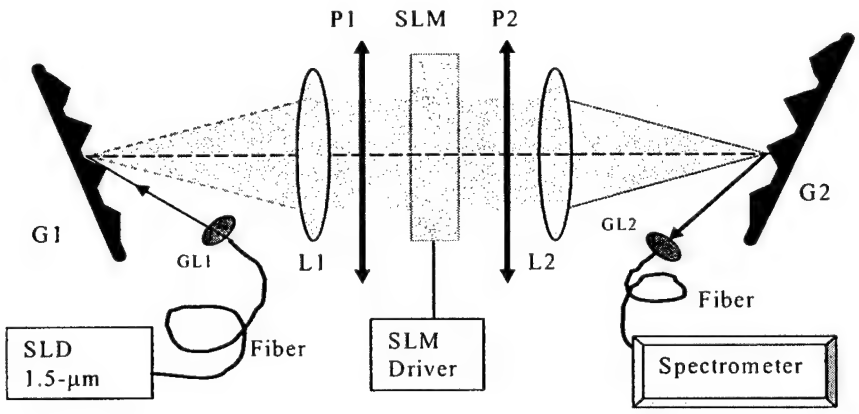


**Fig. 3.1: Spectral encoding of the SLD spectrum via a SLM**

An economical choice of light source for our system was an SLD module, purchased from Dora Texas Corp. However, as a trade-off, more work had to be done at BNS to incorporate the source into the system. A board was designed to accommodate the SLD module, and a separate electronic driver was purchased from Micro Laser Systems Inc, which provides driving current up to 400 mA. The SLD output was then amplified by an EDFA available at BNS to give an output of up to about 40 mW. This has been a very time-consuming process, but finally the SLD module provided a very convenient broadband source with enough output power for decoding experiments.

For a typical test, Figure 3.2(a) shows the original power spectrum (dashed) of a SLD amplified by an EDFA, and the modulated power spectrum (solid) when the LC-SLM strips are set to the coding pattern of alternative on and off driven with equal binary voltages. An un-flattened spectral code of {0101010110101010} is achieved due to the spectral profile of the SLD-EDFA amplified source. When the LC-SLM strips are modulated in an analog way, a uniformed (flattened) spectrum modulation (solid) is achieved as shown in figure 3.2(b), compared with the un-flattened spectrum (dotted). The uniformity of the coding spectrum is greatly improved, which can lead to better performance of the OCDMA system.

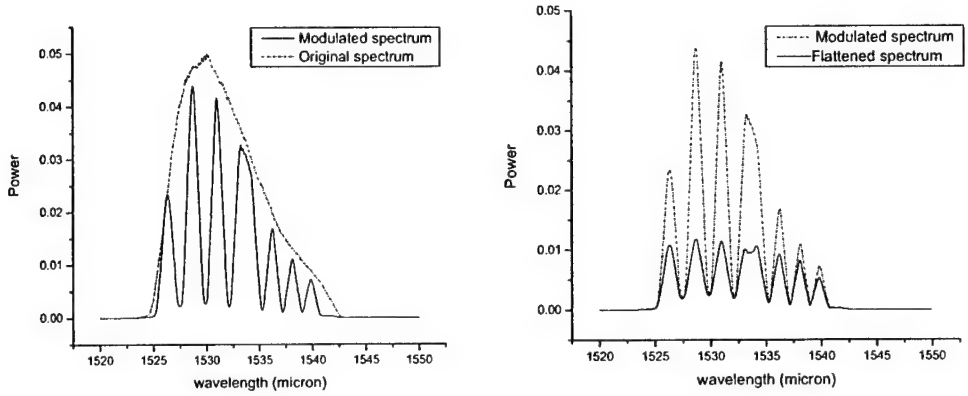


**Fig. 3.2: Original and modulated (un-flattened and flattened) power spectra of the EDFA amplified SLD light via a SLM**

### 3.1.2 Encoding System Analyses

The light source we used in the system is a SLD amplified by an EDFA. The coherent length of this kind of the light source is only a few millimeters, and thus we needed to develop a more general approach than the monochromatic one to analyze the system. We will utilize the mutual coherent function propagation in free space to analyze the transmission characteristics of the optical system. [17]

To describe the source plane and the image plane of the optical system, let $Q_1(\xi_1,\eta_1)$, $Q_2(\xi_2,\eta_2)$ represent two points on the source plane, and $P_1(x_1,y_1)$, $P_2(x_2,y_2)$ represent two points on the image plane, respectively. We also introduce two complex vectors $X=\{x_1,y_1,ix_2,iy_2\}$ and $\rho=\{\xi_1,\eta_1,i\xi_2,i\eta_2\}$ by defining the following:

$$\begin{aligned} X\rho &= x_1\xi_1 + y_1\eta_1 - x_2\xi_2 - y_2\eta_2 \\ X^2 &= x_1^2 + y_1^2 - x_2^2 - y_2^2 \\ \rho^2 &= \xi_1^2 + \eta_1^2 - \xi_2^2 - \eta_2^2 \end{aligned} \qquad (3.1)$$

The mutual spectral density $G$ is the Fourier-transform of the mutual coherent function. The propagation of mutual spectral density between two planes in free space can be described as: [17, 18]

$$G(X,\nu) = \frac{\nu^2}{c^2z^2}\int G(\rho,\nu)\exp[\frac{i\pi\nu}{cz}(X-\rho)^2]d\rho \quad , \qquad (3.2)$$

where ν is the frequency, c is the speed of light, and z is the propagation distance between two planes.

For the propagation of mutual spectral density in the scheme depicted in figure 3.1, let $t_m(x,\nu)$ be the mask transfer function of the SLM and $T_m(X,\nu) = t_m(x_1,\nu)t_m{}^*(x_2,\nu)$, then the mutual spectral intensity at the output can be shown to be:

$$G(\rho',\nu) = \frac{\nu^4}{c^4F^4}\iint G_{in}(\beta\rho,\nu)\beta\exp(i\gamma\Omega(\xi_1-\xi_2))\exp(-i\frac{2\pi\nu}{cF}X\rho)T_m(X,\nu)\exp(-i\frac{2\pi\nu}{cF}X\rho')dXd\rho \qquad (3.3)$$

where, F is the lens focal length, and the mutual coherent function of the incident beam can be written as:

$$G_{in}(\rho,\nu) = \frac{2}{\Delta\nu_0\sqrt{\pi}}\exp(-\frac{(\nu-\nu_0)^2}{(\Delta\nu)^2})\frac{2P^0}{\pi r_V^2}\exp(-\frac{\xi_1^2+\eta_1^2}{r_V^2})\exp(\frac{\xi_2^2+\eta_2^2}{r_V^2}) \quad , \quad (3.4)$$

using a simplified model of the incident beam satisfying Gaussian distribution written in the form of:

$$u(\xi,\eta) = \sqrt{\frac{2P^0}{\pi r_V^2}}\exp(-\frac{\xi^2+\eta^2}{r_V^2}), \qquad (3.5)$$

while $r_V$ is the radius of the incident light beam, $P^0$ is the incident power , $\nu_0$ is the central wavelength and $\Delta\nu$ the bandwidth of the spectrum.

In the equation above, we also used the transfer function of an optical grating for a coherent wave field:

$$E_{out}(x,\omega) = \sqrt{\beta}E_{in}(\beta x,\Omega)\exp(i\gamma\Omega x) \qquad (3.6)$$

where:

$$\beta = \cos(\theta_i)/\cos(\theta_d) \qquad \gamma = 2\pi/\bar{\omega}d\cos(\theta_d) \qquad \Omega = \omega - \bar{\omega}$$

with $\theta_i$ and $\theta_d$ being the incident angle and the diffracted angle, respectively, and d the grating period, $\omega$ the angular frequency, $\overline{\omega}$ the central angular frequency.

We calculated the transmission efficiency for different wavelengths under different SLM pitch sizes. Figure 3.3 shows the results at SLM pitch sizes of 300 μm and 150 μm, respectively. The LC-SLM strips are set to the alternative on–and-off coding pattern, and the following parameters close to the experiment are used:

$$\nu_0 = 1.53\mu m$$
$$\Delta\nu_0 = 10nm$$
$$r_V = 2.5mm$$
$$F = 70mm$$
$$\theta_i = 62^O$$

It can be seen that the modulation depth of the transmitted spectrum increases with the strip width of the LC-SLM. A good modulation extinction ratio can be achieved with a strip width of 300 μm. In our experiments, we typically chose a large strip width of 400 $\mu m$, to ensure good modulation of the power spectrum.

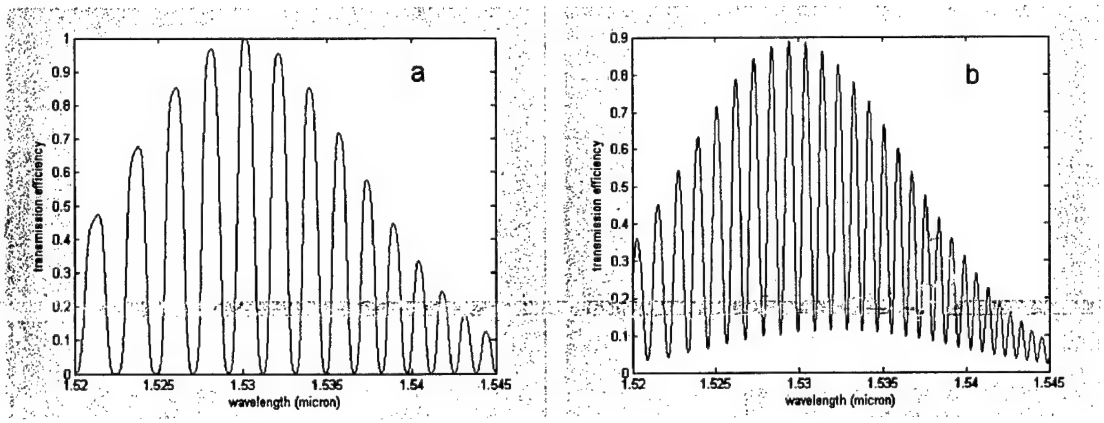


**Fig. 3.3: Transmission characteristics of the encoding system: a): transmission at LC strip width = 300 μm; b): transmission at LC strip width = 150 μm**

## 3.2 Spectrum Decoding

We built a fiber-based spectrum encoder/decoder pair as shown in figure 3.4. The power spectrum of the incoming light beam is divided into 16 slices, or chips, and encoded into J pattern by programming the one-dimensional SLM1 as shown in figure 3.2 for a code pattern of {0101010110101010}. The encoded power spectrum is coupled into a single-mode fiber by a collimation lens and then sent to the decoder via a fiber. The encoded light passes SLM2 with a pattern corresponding to K, the code

selected for detection. With the polarization of J code being 45° (set by the input polarizer) to the axis (vertical) of SLM2, the transmitted light of SLM2 consists of two orthogonal components being +45° and –45° from the SLM2 axis and producing signals proportional to $J \cdot K$ and $J \cdot \overline{K}$, respectively. The two light components are rotated by a polarization rotator (PR) 45° to the perpendicular and parallel polarization state. The beam is then focused by a lens and diffracted by a grating into collimated beams. A polarizing beam splitter (PBS) cube can then separate the two signals proportional to $J \bullet K$ and $J \bullet \overline{K}$ into two beams. These two beams are coupled back into two fibers and measured by photo detectors. When a balanced detection method is used, the photodetector currents are subtracted from each other, and the resulting signal is proportional to the bipolar correlation $\Theta_{XY}$ of Eq. (1.2).

In a local area network, the received signal will be a superposition of spectra corresponding to the entire set of active user's codes. Since the receiver is linear in optical power, the output will be a superposition of their correlations with the desired code. A sequence of signals from the desired user will produce large value $\Theta_{XY}$ or $-\Theta_{XY}$. The interference between the desired user and other users is suppressed using bipolar codes to near zero, or very low magnitude as in Walsh or Gold codes. The high polarization selectivity of these bulk components coupled with the polarization rotation ability of liquid crystal elements makes switching possible with high extinction ratio and low crosstalk.

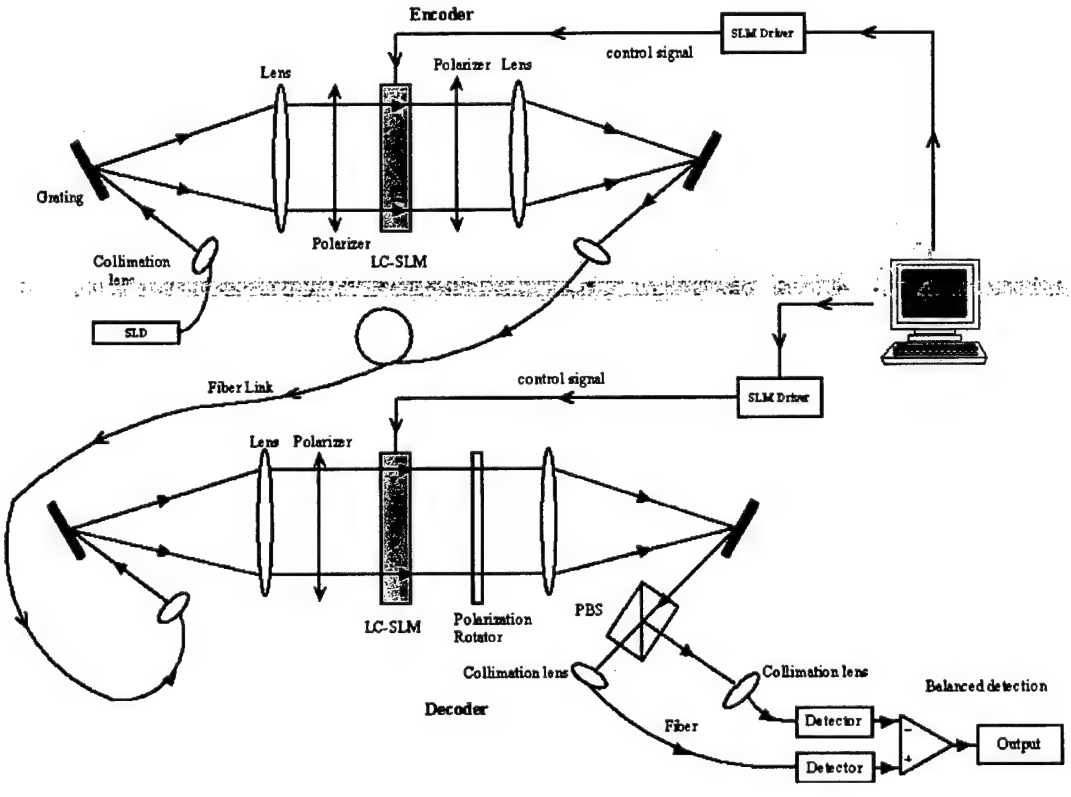


**Fig. 3.4: Fiber-based testbed for spectrum encoding and decoding.**

During the experiment, the two SLMs needed to be aligned spatially with each other to get the same modulation of the power spectrum. To do this, we applied the same code {1010101001010101} to both the encoder and decoder at the same time. By observing the spectrum overlapping of two modulated spectra via a spectrometer, we could tell whether the two LC-SLMs were aligned perfectly with each other. First, we needed to move the LC carefully until the two modulated spectra almost overlapped, as shown in Figure 3.5. Then by (electronically) setting the relative pixel offset position of the two SLMs, they could be aligned conveniently.

After the SLMs were aligned, the power difference of the two orthogonal components following the decoder (signals proportional to $J \cdot K$ and $J \cdot \overline{K}$), i.e. correlation, were measured. Four orthogonal codes (and their conjugates) were chosen: $J1$={11001100 00110011}, $J2$={11110000 00001111}, $J3$={10011001 01100110}, $J4$={01010101 10101010}and their complex conjugates $\overline{J}_1$, $\overline{J}_2$ , $\overline{J}_3$, $\overline{J}_4$. The encoder SLM1 was fixed to code $J_4$, while the coding pattern of the decoder SLM2 varied to transmit any of the code sequences, $J_1$, $J_2$, $J_3$, $J_4$ $\overline{J}_1$, $\overline{J}_2$ $\overline{J}_3$ and $\overline{J}_4$. Figure 3.6 shows the

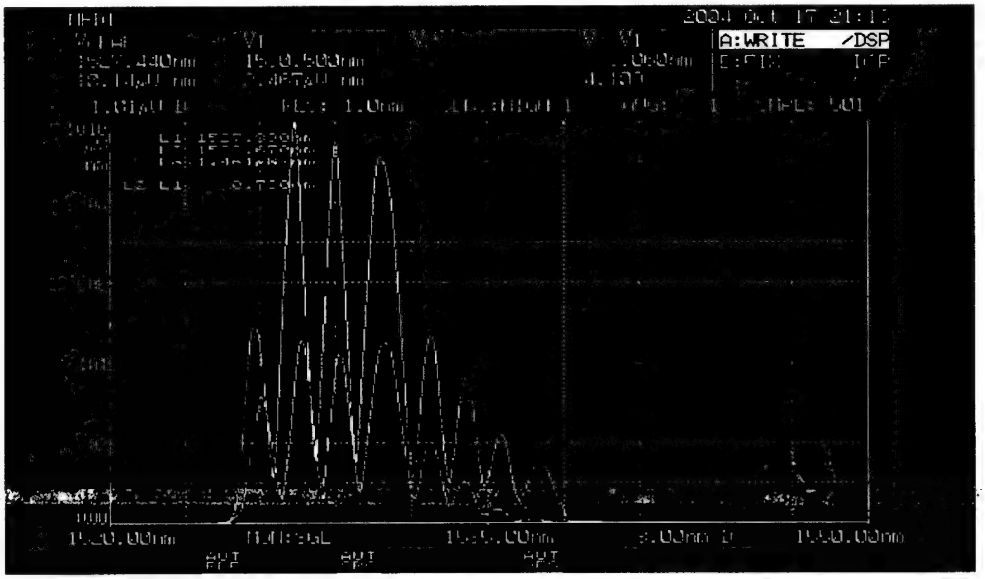


**Fig. 3.5: SLM alignment: almost overlapped spectrum patterns modulated by the encoder (yellow) and decoder (pink, lower peaks).**

auto-correlation and cross-correlation between the codes that were measured when the encoder SLM1 was set to $J4$ with the above single-user configuration (figure 3.4). It can be seen that only when the matched codes $J4$ or $\overline{J}4$ were set for SLM2, the decoder responded with a large positive or negative correlation signal. Good contrast between the autocorrelation and cross correlation values shows that a binary information symbol can be recovered by an appropriate threshold operation, demonstrating the feasibility of encoding and decoding for this fiber-based optical CDMA system.

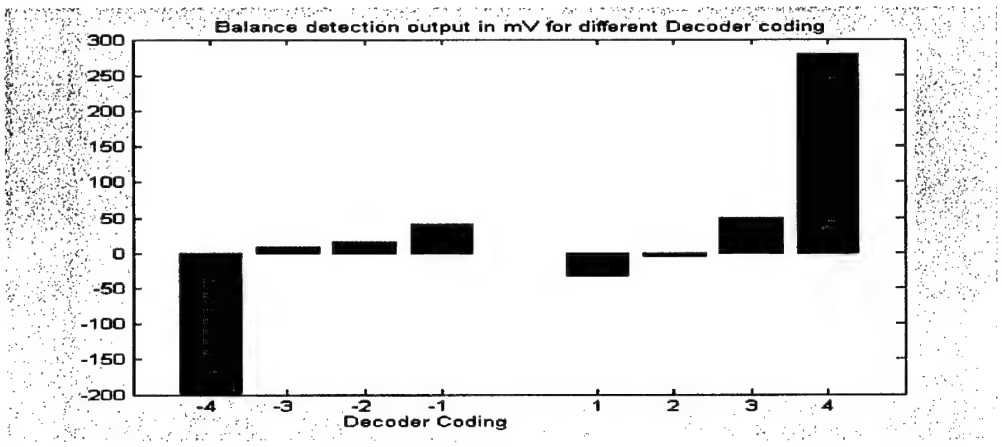


**Fig. 3.6: Measured correlation values of the codes. The encoder SLM1 pattern was fixed as J4, while the decoder SLM2 sent all the patterns sequentially (J1, J2, J3, J4 [1,2,3,4] and their complex conjugates [-1,- 2, -3, -4]).**

## 3.3 Bit Error Rate Testing

Figure 3.7 sketches the schematic fiber testbed used to perform measurements of auto- and cross-correlations, as well as the multiple access interference (MAI) rejection and bit-error rate (BER). The output data from a BER testing (BERT) equipment [a digital analyzer HP 3764A] is sent to the SLD light source controller to modulate the output intensity of the SLD. The SLD working point was carefully tuned to get the optimized intensity modulation. The modulated SLD output beam amplified by an EDFA is then sent into a 50/50 fiber splitter where the light is evenly split and coupled into the two fiber-based encoders. The coded output beams of the two encoders are combined again at another 50/50 fiber coupler. After transmission through the fiber trunk, the mixed optical signal is sent into the decoder via fiber connector for information decoding. By setting the address code at the decoder to be the same as one of the encoder address codes, we were able to decode the information bits out of the mixed signal. The bipolar code detection was performed via a balanced differential detector with signal amplification. The output electrical signal is finally sent to the data input port of the digital analyzer. The digital analyzer measures and reports the BER performance at a certain modulation speed by comparing the data input and data output. An oscilloscope is also connected for signal wave display and analyses.

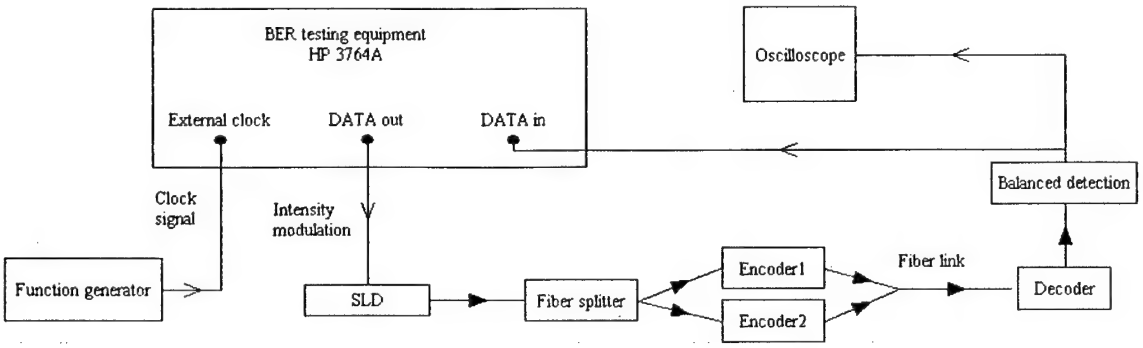


**Figure 3.7: Schematic sketch of a 2-user fiber testbed setup.**

The digital analyzer HP 3764A has a working frequency of 137 MHz. However, our light source (SLD) has a low-speed electronic driver [from Micro Laser Systems Inc.] with a limited maximum modulation speed of 1.5 MHz. We have therefore tested our system at around 1 MHz. To test the BER performance at a modulation speed lower than 137 MHz, we needed to use an external clock signal to drive the BERT equipment. A function generator was connected to the external clock input of the digital analyzer. The output of the function generator was set to be pulse or square wave mode so that it could be recognized as a clock signal at the clock input. The output data speed of the digital analyzer was the same as the external clock signal. We then changed the data speed of the digital analyzer by tuning the speed of the external clock speed. The output data format could be set by the digital analyzer control panel.

The two encoders can add reconfigurable address codes onto the input information without changing the input signal in time domain. This provides convenience for our various testing purposes. For example, orthogonal codes can be added on the two encoders so that we can observe the MAI rejection of the system. To test the MAI rejection, we first test the one-user configuration as in Figure 3.4 by disabling either of the two encoders. When one of the encoders (e.g. Encoder2) is disabled, there is only one encoder1/decoder transmission pair in the system in Figure 3.7. The codes at encoder 1 and decoder are set to be the same and orthogonal to each other, respectively, so that we can see the difference for autocorrelation and cross-correlation. The result on the oscilloscope is shown in the figure below (Fig. 3.8):

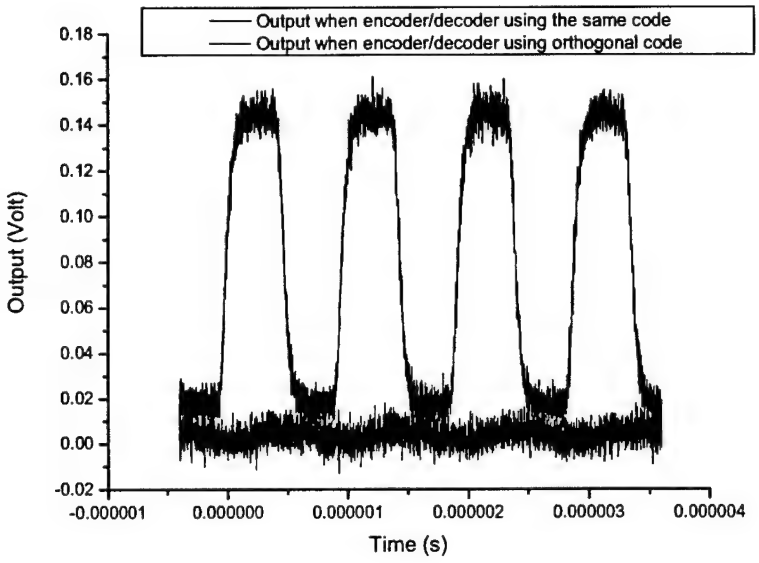


**Fig. 3.8: Measured auto correlation (black) and cross correlation (red) values of the codes when one of the two encoders is disabled.**

The data output at the digital analyzer is set to be [1010...] alternatively, thus from the oscilloscope we can see the decoded information bits as "1010..." in correspondence. The black line shows the decoded information bits, while the red line shows the output when the encoder and decoder are set to be orthogonal to each other. The testing modulation speed is 1MHz. The autocorrelation Peak-Peak value is measured to be 150 mV, while the cross-correlation Peak-Peak value is 10 mV. Thus the signal from other users can be easily rejected by threshold detection, as discussed in Section 3.2. This testing set the encoder1/decoder in the optimized position. We then did similar testing for the encoder2/decoder pair by disabling encoder1, and setting encoder2/decoder to the optimized position.

After the 2-user (encoders 1 and 2) configuration was optimized, we tested the MAI rejection performance of our optical CDMA system. Both encoders are enabled, but with orthogonal codes added with each other. The address code of the decoder is set to be the same as one of the encoder. Then the other encoder plays the role of an interference user. The testing result based on Figure 3.8 is shown in the table below together with BER measurements:

| | Without MAI | With MAI |
|---|---|---|
| Autocorrelation | 150 mV | 110 mV |
| BER | 0 | 0 |

From the testing result, we can see that with the existence of MAI, the autocorrelation Pk-Pk value did decrease. However, this value is still well distinguishable from the cross-correlation, and the BER result from the digital analyzer is 0 as well. For an optical CDMA network, different users share the same wavelength, time slot and transmission medium. Only address codes are used to discriminate between different users. Thus the rejection of MAI (multiple-access-interference) is a major limiting factor for the performance of an optical CDMA network. The above testing for MAI rejection and BER performance demonstrates the potential capability of our OCDMA system.

## 3.4 Mechanical Design and Packaging

After the final opto-mechanical design for housing the OCDMA system was completed, we built two compact aluminum boxes; one (Figure 3.9) for housing the two identical encoders and one (Figure 3.10) for the decoder. All the optical components and SLMs were integrated into a compact mechanical system. FC/PC fiber connectors were mounted on the box panel for light signal input/output through single-mode fibers.

Figure 3.9 shows the packaged structure for the two encoders assembled in parallel, together with the encoder sketch shown on the top (only one encoder setup is shown). To reduce the polarization loss, two polarization rotators [at 45 degrees rotation, not drawn in Figure 3.9(a)] were used in conjunction with the polarizers. All the optical components are mounted on the mirror mounts (either commercial or customized) fixed on the aluminum sliding base.

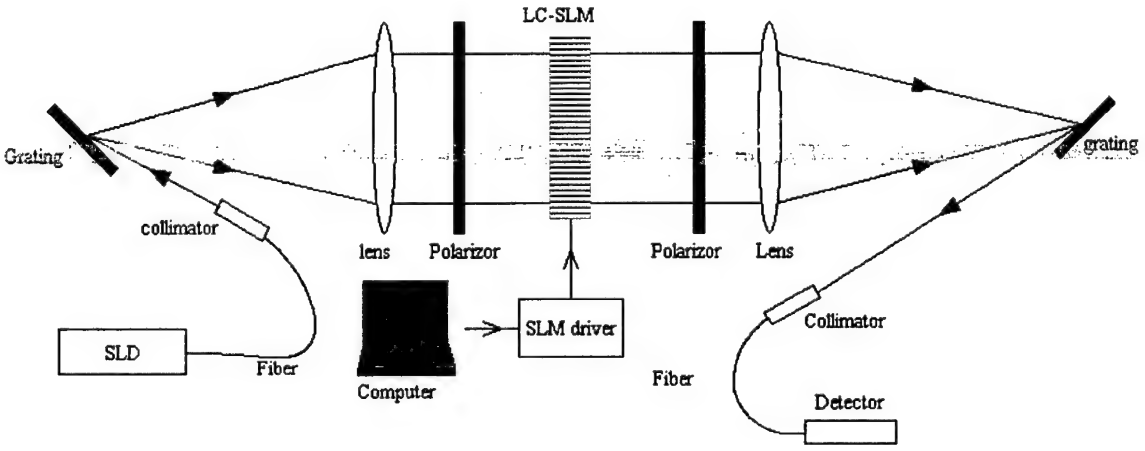


**Fig. 3.9(a): A sketch of a fiber-based encoder.**

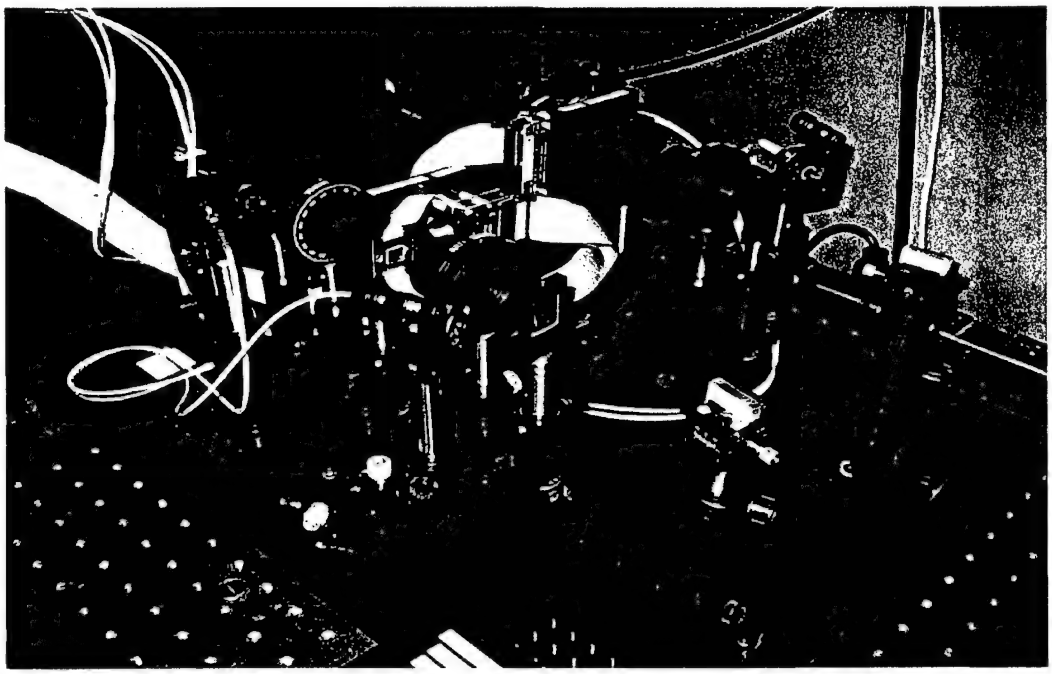

**Fig. 3.9(b): Two fiber-based encoders packaged in parallel for spectrum encoding.**

Figures 3.10(a) and 3.10(b) show the schematic and mechanical assembly for the decoder. It is very similar to the encoder except that a polarization beam splitter (PBS) is used for splitting the two sets of conjugated coding patterns into two beams with orthogonal directions, which are collected onto two separate IR photo detectors, producing signals proportional to $J \cdot K$ and $J \cdot \overline{K}$, respectively.

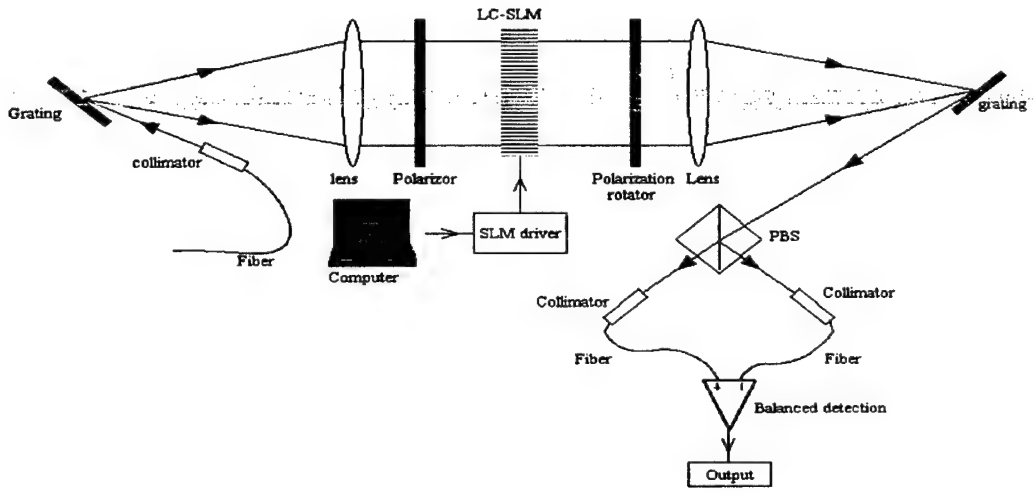


**Fig. 3.10(a): Sketch of fiber-based decoder.**

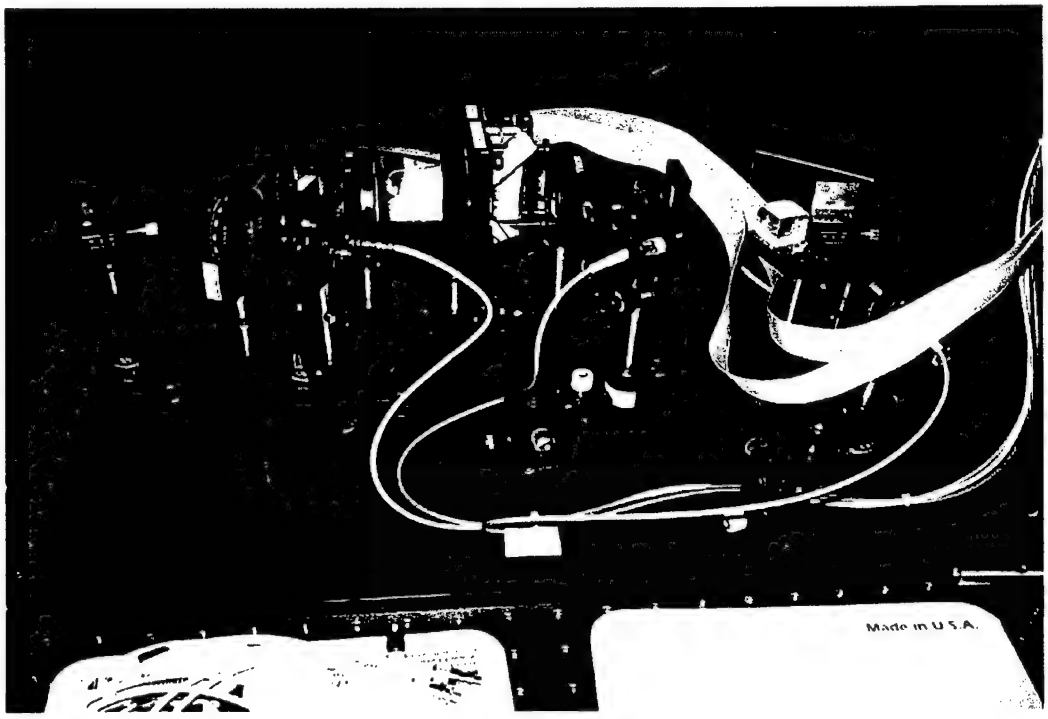


**Fig. 3.10(b): Fiber-based decoder packaged for spectrum decoding.**

Figure 3.11 pictures the whole 2-user OCDMA system. This is the first prototype commercial product. Two fiber inputs to the encoder box give two encoded patterns for output signal beams via the fibers. A 2x1 fiber cable can then combine these two outputs into a single fiber for transmission across long distances. On the decoder side, one fiber input and two fiber output connectors are built into the panel. The encoded pattern input is decoded by measuring the correlations via a balanced detection of the two fiber output signals. The resulting electrical signal is proportional to the bipolar correlation $\Theta_{XY}$ of Eq. (1.2).

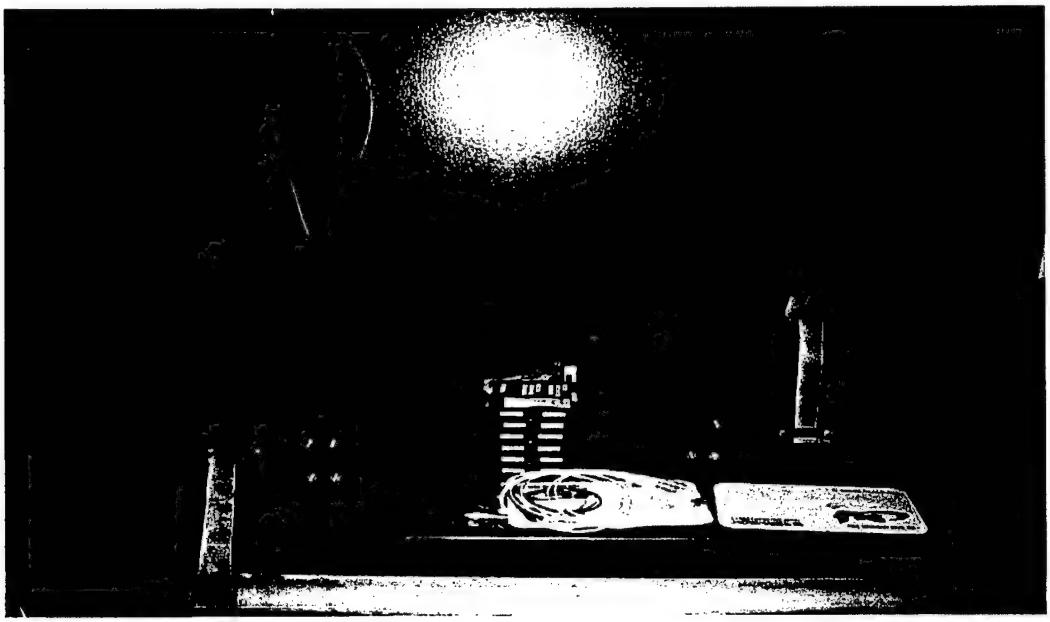

**Fig. 3.11: Photograph of the 2-user OCDMA prototype including two encoders (left) and one decoder (right). The middle stacks are 3 electronic boxes controlling the 3 arrayed SLMs via USB connection.**

# 4 OCDMA Noise Analyses

We have done some theoretical work to simulate the noise characteristics of the OCDMA system. In this chapter we will present the basic formalism and a preliminary result of the noise analysis of the OCDMA system containing SLM modulation. Both the beat noise and shot noise are taken into consideration.

## 4.1 Formalism

Assume we use M-sequence code for the spectral-amplitude modulation of the optical CDMA system. For ideal M-sequence code, we have:

$$\sum_{i=1}^{N} C_k(i)C_l(i) = \begin{cases} (N+1)/2 & k = l \\ (N+1)/4 & k \neq l \end{cases} \qquad (4.1a)$$

$$\sum_{i=1}^{N} C_k(i)\overline{C_l}(i) = \begin{cases} 0 & k = l \\ (N+1)/4 & k \neq l \end{cases} \qquad (4.1b)$$

In the equations above, $C_k$ is the code used by the kth-user of the network, and $\overline{C_k}$ is its orthogonal code, $N$ is the code length used for the system.

However, the assigned code for each user is not the ideal code in our optical system. The triangle function is found to be more close to our real case, and will be assumed for our initial simulation. Then the cross-correlation and self-correlation characteristic for the code should be:

$$\sum_{i=1}^{N} C_k(i)C_l(i) = \begin{cases} (N+1)/2 & k = l \\ (N-1)/2 & k \neq l \end{cases} \qquad (4.2a)$$

$$\sum_{i=1}^{N} C_k(i)\overline{C_l}(j) = \begin{cases} (N+1)/4 & k = l \\ (N-3)/4 & k \neq l \end{cases} \qquad (4.2b)$$

Assume all the power spectrum slices contain the same energy, and consider the worst case that all users are sending "1" at the same time (using OOK for the information

transmission), the power spectra of the current $I_1$ and $I_2$ at the two detectors are: [19]

$$G_{I_2}(\nu) = \frac{P_{sr}}{\Delta\nu}\sum_{l=1}^{N}\sum_{i=1}^{N} C_k(i)C_l(i)\{u(\nu_k) - u(\nu_l)\} \qquad (4.3a)$$

$$G_{I_2}(\nu) = \frac{P_{sr}}{\Delta\nu}\sum_{l=1}^{N}\sum_{i=1}^{N} C_k(i)\overline{C_l}(i)\{u(\nu_k) - u(\nu_l)\} \qquad (4.3b)$$

To calculate the statistical characteristic of the detected light at the receiver, the variance of the photocurrent from a thermal-like polarized source at the detector is given by Refs [19] and [20]: [19, 20]

$$< I_1^2 >= 2eB\overline{I_1} + B\tau_c(\overline{I_1})^2 \qquad (4.4a)$$

$$< I_2^2 >= 2eB\overline{I_2} + B\tau_c(\overline{I_2})^2 \qquad (4.4b)$$

In the calculation above, thermal noise due to the electrical circuit is not included for calculation simplicity.

From the pdf function of the detector current we can get:

$$\overline{I}_2 = R\int_0^{\infty} d\nu \times G_{I_2}(\nu) = RP_{signal} \times \frac{N-1}{2} \qquad (4.5a)$$

$$\overline{I}_1 = R\int_0^{\infty} d\nu \times G_{I_1}(\nu) = RP_{signal} \times \frac{N-1}{4} \qquad (4.5b)$$

While R is the responsibility of the detector, $P_{signal}$ is the signal power from each user.

For our optical system measuring the difference of two photocurrents from two photoreceivers, the detected current is:

$$I_{dec} = I_2 - I_1 \tag{4.6}$$

And its variance is:

$$\sigma_I^2 = \sigma_{I1}^2 + \sigma_{I2}^2 \tag{4.7}$$

The SNR is $I_{dec}/\sigma_I$ .

## 4.2 Noise Analyses of the System

Using the parameters below:

$B = 155MHz$ $\quad e = 1.6\times10^{-19}C$

$\tau_c = 10^{-13}s$ $\quad R = 0.5$

The relationship between the number of active user and the SNR is shown in Figure 4.1. Figure 4.2 shows the SNR dependence on the signal power when the active user number is set to 60. Both the results for ideal M-sequence code and triangular M-sequence code are included in the figure. As we can see from the results, the signal power for each user will not affect the SNR when reaching a certain power level. Also as we can expect, the calculated SNR is higher for ideal M-sequence code compared with the assumed triangular M-code, simply because the triangular code is just no longer orthogonal with each other, as in the ideal M-code case.

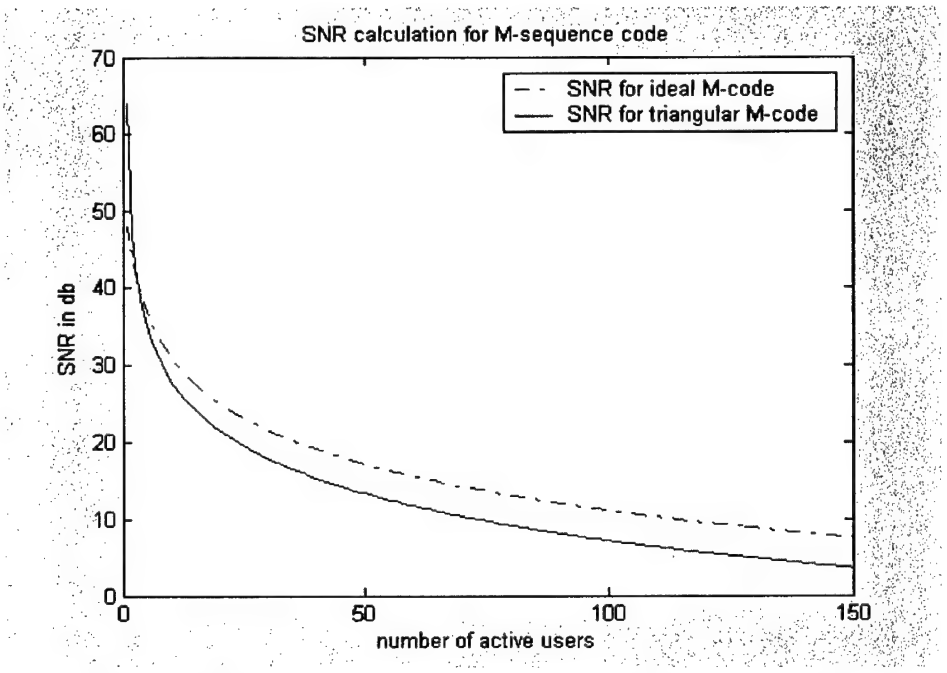


**Figure 4.1: SNR dependence on the number of active users.**

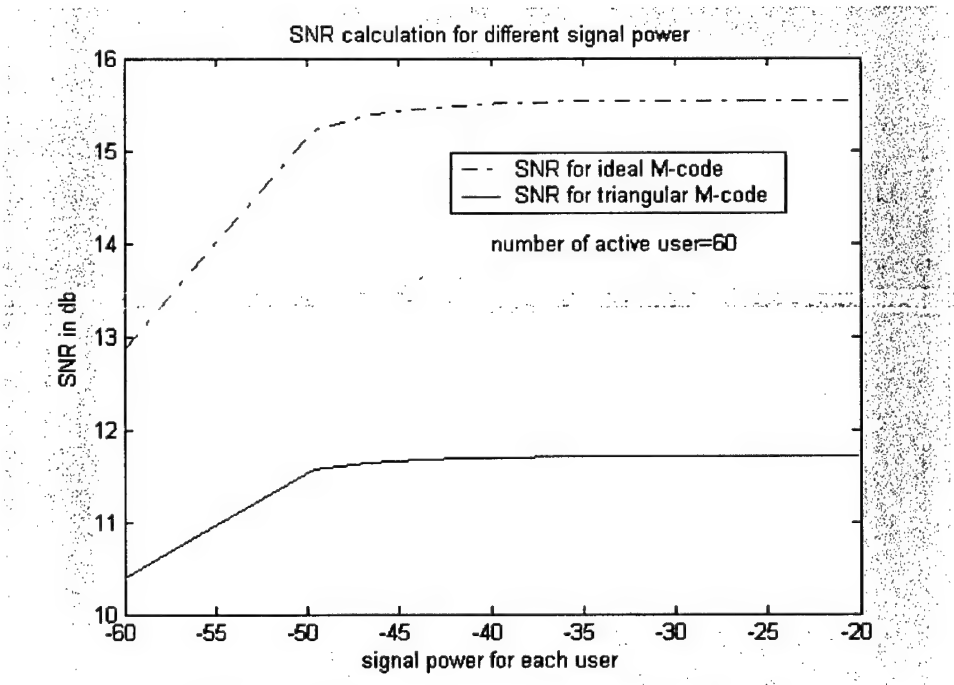


**Figure 4.2: SNR dependence on the signal power.**

# 5 Summary

In Phase II, using liquid crystal spatial light modulators (SLMs), BNS and CU-Boulder have successfully developed bipolar coding techniques in the optical spectral domain for incoherent optical code division multiple access (CDMA) communication. We have fabricated a reconfigurable 2-user encoder-decoder system based on a fiber test-bed using three arrayed LC SLMs. A broadband Super Luminescent Diode source amplified by an EDFA has been spectrally encoded and decoded. The bipolar correlations of the codes are verified. Good contrast between the autocorrelation and cross correlation values shows that a binary information symbol can be recovered by an appropriate threshold operation. BER (bit-error-rate) measurements also show the ability of our system for MAI (multiple-access-interference) rejection.

Important results (milestones) achieved during Phase II are summarized as follows:

(1) Successfully fabricated three analog arrayed (1x64) LC SLMs and developed the controlling software, which is key to encoding and decoding in the optical CDMA system. An analog driving scheme for the SLMs has been employed for uniform coding modulation.

(2) A modulation and detection method was realized that allows all-optical implementation of the bipolar codes and correlation detection. Fiber-based bipolar encoders were demonstrated, showing good linear spectral-spatial-spectral conversion. Good encoded beam in a single mode fiber was obtained.

(3) Fiber testbed of a 1-D Optical CDMA system has been demonstrated with arrayed SLMs. The autocorrelations and cross correlations were measured, and good contrast between the autocorrelation and cross correlation values shows that a binary information symbol can be recovered by an appropriate threshold operation. The system BER and MAI were also measured at the modulation speed of 1 MHz. The system showed good capability for multiple-access-interference rejection.

(4) Successfully packaged the first code-reconfigurable fiber-based prototype OCDMA system using LC SLM spectral modulation.

(5) Performed theoretical analyses of the optical system based on the partial coherency propagation theory. The basic formalism and preliminary results of the noise analysis of the OCDMA system containing SLM modulation are presented. Both the beat noise and shot noise are taken into consideration.

(6) Published two articles at the SPIE proceedings.

For future direction, one obvious task is to test the BER and MAI at much higher modulation speeds, e.g. 1.25 Gb/s (OC-24) or 2.5 Gb/s (OC-48), which was not carried out in Phase II due the limited budget. The main modification will be purchasing a high speed electronic driver for the SLD broadband sources so that the SLD intensity can be modulated at the OC-24 or OC-48 speed. A 10 GB high speed BERT device can be used for BERT testing. This will bring the current prototype to a more practical level for optical communications.

# *Technical References*


1. A. Weiner, J. Heritage, and J. Salehi, "Encoding and decoding of femtosecond pulses," *Opt. Lett.*, **13**, p.300, (1988).

2. D. D. Sampson, G. J. Pendock, and R. A. Griffin, "Photonic code-division multiple-access communications, " *Fiber and Integ. Opt.* , **16**, p.129, (1997).

3. K. Sayano, I. Nguyen, and J. K. Chan, "Demonstration of multi-channel optical CDMA for free space communications, " in *Free-Space Laser Communication Technologies XIII, Proc. SPIE*, **Vol. 4272**, p.38, (2001).

4. Paul R.Prucnal, Mario A. Santoro, Ting Rui Fan, "Spread spectrum Fiber-Optic Local Area Network Using Optical Processing," *J. of Lightwave Tech.*, **LT-4**, p.547, (May 1986).

5. H.P. Sardesai, C.-C. Chang, and A.M. Weiner, "A femtosecond code-division multiple-access communication system testbed," *Journal of Lightwave Technology*, **16**, pp.1953-1964, (1998).

6. A. Grunnet-Jepsen, A. E. Johnson, E. S. Maniloff, T. W. Mossberg, M. J. Munroe, and J. N. Sweetser, "Demonstration of all-fiber sparse lightwave CDMA based on temporal phase encoding," *IEEE Photon. Tech. Letts.*, **11**, pp.1283-1285, (1999).

7. L. R. Chen and P. W. E. Smith, "Demonstration of incoherent wavelength-encoding/time–spreading optical CDMA using chirped moiré gratings," *IEEE Photon. Tech. Letts.*, **12**, p.1281, (2000).

8. T. Ohtsuki, K. Sato, I. Sasase, and S. Mori, "Direct-detection optical synchronous CDMA systems with double optical hard-limiters using modified prime sequence codes," *IEEE J. Sel. Areas Commun.*, **14**, p.1879, (1996).

9. M. Kavehrad, and D. Zaccarin, "Optical code-division-multiplexed systems based on spectral encoding of noncoherent sources," *J. of lightwave Tech.*, **13**, p.534, (1995).

10. L. Nguyen, T. Dennis, B. Aazhang, and J. F. Young, "Experimental demonstration of bipolar codes for optical spectral amplitude CDMA communication," *J. of Lightwave Tech.*, **15**, p.1647, (1997).

11. T. Dennis and J. F. Young, "Experimental demonstration of bipolar codes for optical spectral amplitude CDMA communication," *IEEE J. of Quantum Electron.*, **35**, p.287, (1999).

12. T. Dennis and J. F. Young, "Measurements of BER performance for bipolar encoding of SFS," *J. of Lightwave Tech.*, **17**, p.1542, (1999).

13. C. H. Eyoh and L. Zhang, "Transmission of ATM cells over optical CDMA links," *Electron. Letts.* **32**, p.2168, (1996).

14. Steve A. Serati and Kipp A. Bauchert, "Analog spatial light modulators advances and applications," in *Spatial light modulators*, *Proc. SPIE*, **Vol. 3292**, (1998).

15. Kipp A. Bauchert, Steve A. Serati and Alex Furman, "Advances in liquid crystal spatial light modulator ," in *Optical Pattern Recognition XIII*, David P. Casasent, Tien-Hsin Chao, Editors , *Proc. SPIE*, **Vol. 4734**, p35, (2002).

16 R. B. Meyer, L. Liebert, L. Strzeleki and P. Keller, "Ferroelectric liquid crystals," *J. Phys. Lett.* (Paris) **36**, 69, (1975).

17. V. Morozov, J. Neff, and H. Zhou, "Signal and noise analysis in free-space interconnects," *J. Opt. Soc. Am. A*, **14**, p. 859, (1997).

18. Marc M. Wefers and Keith A. Nelson, "Space-Time Profiles of Shaped Ultrafast Optical Waveforms," *IEEE J. of Quantum Electronics*, **32**, p. 161, (Jan 1996).

19. Zou, Shalaby, and Ghafouri-Shiraz, *J. Lightwave Technol.* Vol. **19**, No. 9 (Sept 2001).

20. J.W. Goodman, Statistical Optics, John Wiley, (2000).

21. Xiao-Wei Xia, Teresa K. Ewing, Steven A. Serati, Yijing Fu, Rong Zhou, John A. Neff, and Frank S. Barnes, "Demonstration of reconfigurable O-CDMA using liquid crystal modulators," in *Active and Passive Optical Components for WDM Communications III*, Achyut K. Dutta, Abdul Ahad S. Awwal, Niloy K. Dutta, Kazuo Fujiura, Editors, *Proc. SPIE*, Vol. **5246** (2003), Pp.95-102.

22. Y. Fu, F. Barnes, T. K. Ewing, S. A. Serati, and X-. W. Xia, "Liquid crystal modulated optical CDMA in a fiber-based testbed," in *Active and Passive Optical Components for WDM Communications IV*, Achyut K. Dutta, Abdul Ahad S. Awwal, Niloy K. Dutta, Yasutake Ohishi, Editors, *Proc. SPIE*, Vol. **5595** (2004), Pp.302-309.

# *Appendix: SPIE Publications*

Two papers [21, 22] have been published on the SPIE proceedings, which are attached here for references. We are very grateful to the excellent management by program manager Dr. Jon Sjogren and generous funding through Air Force Office of Scientific Research (AFOSR) Contract F49620-02-C-0021.